E2F1 interacts with BCL-xL and regulates its subcellular localization dynamics to trigger cell death

DOI:
10.15252/embr.201744046

Document Version
Accepted author manuscript

Published in:
EMBO reports

E2F1 interacts with BCL-xL and regulates its subcellular localization dynamics to trigger cell death

Céline Vuillier[1], Steven Lohard[1], Aurélie Fétiveau[1], Jennifer Allègre[2], Cémile Kayaci[2], Louise E. King[3], Frédérique Braun[1,&], Sophie Barillé-Nion[1], Fabien Gautier[1,4], Laurence Dubrez[2], Andrew P. Gilmore[3], Philippe P. Juin[1,4]* and Laurent Maillet[1]*

[1] CRCINA, INSERM, U1232, Université de Nantes, Nantes, France
[2] LNC, INSERM, UMR866, Université de Bourgogne Franche-Comté, Dijon, France.
[3] Wellcome Centre for Cell-Matrix Research, Faculty of Biology, Medicine and Health, Manchester Academic Health Sciences Centre, University of Manchester, Manchester, UK.
[4] ICO René Gauducheau, Saint Herblain, France
[&] current adress : CNRS UMR8261, Institut de Biologie Physico-Chimique, Paris, France.
* co-corresponding authors

Character count (excluding references and materials and methods): 26671

GRAPHICAL ABSTRACT

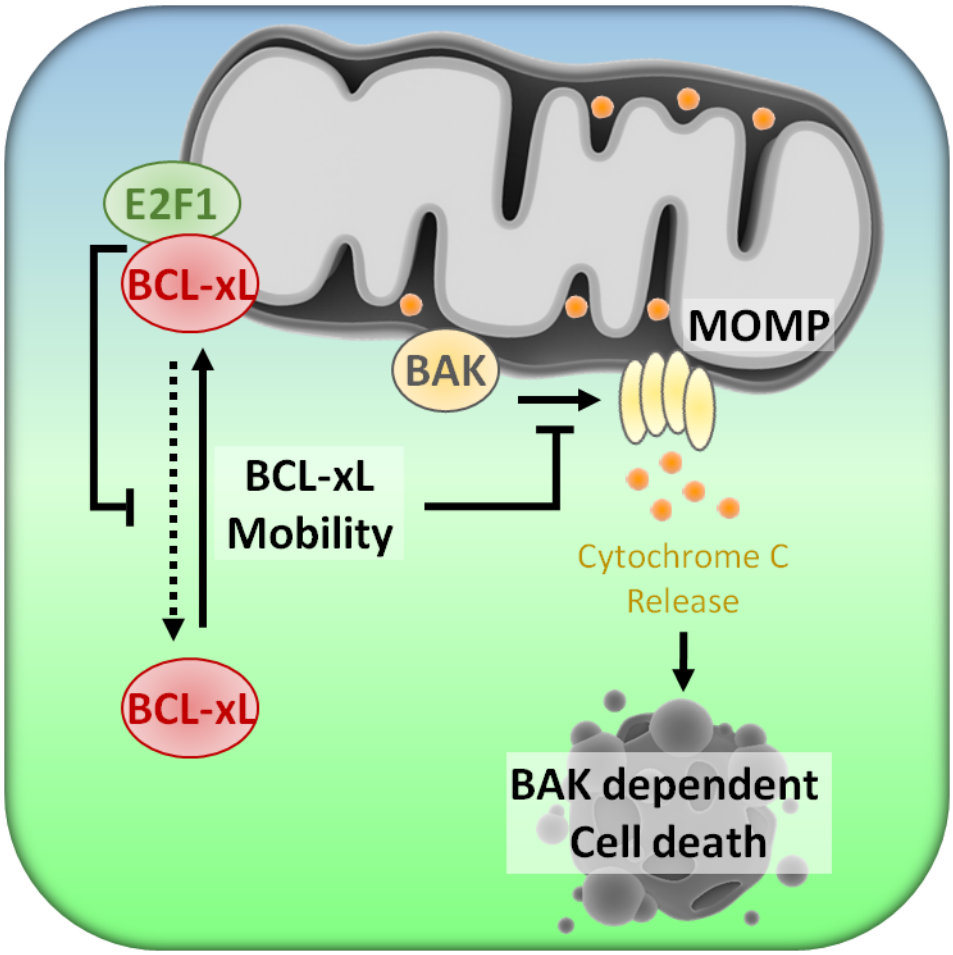

HIGHLIGHTS

- E2F1 exerts a non transcriptional pro-apoptotic function at the mitochondria
- E2F1 interacts with BCL-xL
- E2F1 negatively regulates BCL-xL mobility
- BCL-xL mobility is required for efficient BAK dependent cell death inhibition

Running title: E2F1-BCL-xL interaction triggers apoptosis
Keywords: E2F1; apoptosis; BCL-2 family; BCL-xL mobility

Short summary:
Vuillier et al. highlight that E2F1 interacts with BCL-xL, independently from its BH3 binding groove, and decreases the subcellular mobility of BCL-xL. This interferes with its ability to inhibit mitochondrial outer membrane permeabilisation and accounts for transcription independent E2F1 induced apoptosis.

ABSTRACT

E2F1 is the main pro-apoptotic effector of the pRB regulated tumor suppressor pathway by promoting the transcription of various pro-apoptotic proteins. We report here that E2F1 partly localizes to mitochondria, where it favors mitochondrial outer membrane permeabilization. E2F1 interacts with BCL-xL independently from its BH3 binding interface, and induces a stabilization of BCL-xL at mitochondrial membranes. This prevents efficient control of BCL-xL over its binding partners, in particular over BAK resulting in the induction of cell death. We thus identify a new, non BH3-binding regulator of BCL-xL localization dynamics that influences its anti-apoptotic activity.

INTRODUCTION

Major tumor suppressor pathways, such as those relying on p53 or pRB/E2F1, promote pro-apoptotic signals that ultimately converge on Mitochondrial Outer Membrane Permeabilization (MOMP) [1]. BCL-2 (B-cell lymphoma/leukemia-2) family proteins are critical regulators of this process [2–4]. They are classified into three functionally distinct subgroups depending on their BCL-2 homology (BH) domain composition: multidomain anti-apoptotic proteins (BCL-xL, BCL-2, MCL-1…) oppose multidomain pro-apoptotic proteins (BAX, BAK) and their upstream effectors the BH3-only pro-apoptotic members (BAD, BIM, BID, NOXA, PUMA…) [5]. They do so in great part by engaging in a network of physical interactions, in which the BH3 domain of pro-apoptotic proteins is bound to the hydrophobic groove at the surface of anti-apoptotic proteins. The balance between these different interactions determines whether or not MOMP occurs due to BAX/BAK oligomerization in mitochondrial membranes.

Changes in BCL-2 protein complexes that lead to MOMP in response to tumor suppression have been extensively described. Not only p53 transcriptionally regulates the expression of BH3-only proteins but it also acts through a non transcriptional effect: it indeed localizes to mitochondria [6] where it can interact with anti-apoptotic BCL-2 proteins [7] or with BAX to directly activate it [8]. Therefore p53 exerts a widespread effect on mitochondrial apoptotic priming by impacting, in many ways, on the composition and assembly of the BCL-2 network [9]. Several BCL-2 proteins including BAK and BCL-xL localize preferentially at intracellular membranes (especially in the outer mitochondrial membrane) due to a hydrophobic C-terminal anchor [10]. The current view is that competence to die can be inferred by snapshot analysis of the state of the BCL-2 network at mitochondria [11]. However, recent data have highlighted that more dynamic features may also intervene. At a whole cell level, BAX, BAK and BCL-xL are not only targeted to mitochondria but their outer membrane associated and integral forms are also shuttled back (« retrotranslocated ») at varying rates [12]. Retrotranslocation of pro-apoptotic proteins protects from cell death [13–15]. In contrast, the mechanisms of BCL-xL retrotranslocation and its impact on MOMP onset are not yet completely understood.

E2F1 is the main pro-apoptotic effector of the pRB regulated tumor suppressor pathway. It was described to promote p53 dependent and independent apoptosis in response to either oncogenic stress or DNA damage [1]. E2F1 is recognized to mainly function as a transcription factor, inducing the expression of numerous pro-apoptotic actors, including some BH3-only proteins such as PUMA and BIM. Its transcriptional

activity is negatively regulated by pRB in most cases, even though positive modulation was reported upon genotoxic and apoptotic stress [16,17]. Because some reports hinted that E2F1 might also promote apoptosis by transcription independent mechanisms [18,19], we herein investigated whether it might exert a direct effect on the mitochondrial BCL-2 network, as was reported for p53 and for its binding partner pRB [7]; [20]. We herein show that E2F1 physically interacts with BCL-xL and that it inhibits BCL-xL localization dynamics, which we establish here as critical for negative regulation of MOMP.

RESULTS & DISCUSSION

E2F1 pro-apoptotic activity relies on its stabilization at the protein level in response to cell death stimuli, such as DNA damage, resulting in numerous post-translational modifications [17]. Consistent with this, treatment of pRB deficient, p53-null Saos-2 cells with the genotoxic agent etoposide, at a concentration that induced apoptosis, enhanced E2F1 expression (Fig 1A). E2F1 contributed to cell death induction, since down regulation of its expression by siRNA significantly decreased etoposide induced cell death rates (Fig 1B). Subcellular fractionation Saos-2 cells (Fig 1C) and of other cell types (Fig EV1A), based on differential centrifugations, revealed the presence of endogenous E2F1 in the heavy membrane fraction that includes mitochondrial and reticulum endoplasmic markers. Mitochondrial fractions with reduced endoplasmic reticulum markers obtained by a second approach based on magnetically labeled anti-TOM22 antibody showed enriched E2F-1, further highlighting its mitochondrial localization (Fig 1C).

We investigated whether E2F1 would contribute to apoptosis when localized at intracellular membranes, and specifically at mitochondria. We engineered a mitochondrial targeted, GFP-fused wild type E2F1 (GFP-E2F1, hereinafter named wt form) to which was fused the mitochondrial targeting sequence of ornithine carbamoyltransferase (OTC-GFP-E2F1, hereinafter named OTC form), using a strategy previously used to investigate the mitochondrial effects of p53 and pRB [6,20] (Fig EV1B and Appendix Fig S1A). Specific mitochondrial targeting of OTC-GFP-E2F1 was confirmed by fluorescence microscopy (Fig EV1C). We investigated pRB and p53 independent biological effects of mitochondrial targeted E2F1 by transient transfection of Saos-2 cells followed by investigation of GFP positive cells. As shown in figure 1D, enhanced expression of either wt or OTC forms was sufficient per se to trigger cell death. Importantly, both E2F1 forms sensitized Saos-2 cells to etoposide-induced cell death, strongly arguing that mitochondrial E2F1 potently contributes to cell death onset (Fig 1D). As previously published [6], targeting GFP to mitochondria using OTC did not induce cell death (Fig EV1D). Ectopic expression of wt or OTC E2F1 forms induced caspase 3 activation and triggered caspase-dependent cell death since the pan-caspase inhibitor Q-VD-OPh completely protected cells (Fig EV2A-B). To directly investigate whether enhanced E2F1 expression triggers MOMP, we used the reporter breast cancer cell line MDA-MB231 that stably expresses an OMI red fluorescent fusion protein which is degraded by the proteasome when released from mitochondria following MOMP [21] (Fig EV2C). Quantitative assays by cytometry based on red fluorescence intensity of mitochondria allowed us to discriminate, among GFP- positive cells, intact cells from cells that underwent MOMP (Fig EV2D). Both wt and OTC forms triggered MOMP (as detected by a decrease in red fluorescence intensity of mitochondria) in these cells and annexin V staining (Fig 1E and EV2E).

As expected, transient transfection of OTC-GFP-E2F1 had no detectable effect on mRNA expression of E2F1 canonical pro-apoptotic transcriptional targets such as TP73, PUMA/BBC3 or BIM/BCL2L11, whose

expression was induced by GFP-E2F1 in control experiments (Fig EV2F). In addition, it had no impact on HRK expression, which was reportedly induced by wt E2F1, via the indirect inhibition of a repressor complex [22]. To further substantiate that the apoptotic effects of mitochondrial E2F1 reported above ensue, at least in part, from transcription independent mechanisms, we used GFP-fused E2F1 E132 (named E132 form), a DNA binding defective mutant (Fig EV1B and Appendix Fig S1A) [23]. This E2F1 transcription deficient form induced MOMP and apoptosis by itself and it sensitized Saos-2 cells to etoposide treatment (Fig 1D-E). Likewise, a mitochondrial targeted transcription deficient E2F1 mutant (OTC-GFP-E132) also induced apoptosis upon overexpression (Fig EV1D).

Down regulation of BAK and/or BAX expression by RNA interference showed that death induced by wt and OTC forms relied preferentially on BAK in Saos-2 cells (Fig 2A and Appendix Fig S1B). This was consistent with the identities of anti-apoptotic proteins that prevented cell death induced by either form of E2F-1: ectopic BCL-xL and MCL-1 but not BCL-2 (which does not to modulate BAK dependent cell death, most likely as a result from its lack of interaction with this pro-apoptotic protein) promoted survival (Fig 2B and Appendix Fig S1C). BH3 binding activity was required for BCL-xL to inhibit E2F1-induced cell death, since the BCL-xL R139D mutant, whose BH3 binding is impaired [24](see also below), did not protect cells in the same settings. Moreover, treatment with the BH3 mimetic inhibitor WEHI-539 (which specifically targets BCL-xL) reverted the protection afforded by overexpressed BCL-xL against E2F1 induced cell death (Fig 2B). Consistent with above data, both E2F1 forms (and the E132 form) drastically enhanced the pro-apoptotic effects of ectopically expressed BAK (Fig 2C, EV3 and Appendix Fig S1D). Notably, we also observed a similar sensitizing effect of wt and OTC fused E2F1 upon overexpression of BAX and of the upstream activators, the BH3-only proteins BIM, PUMA and truncated BID (tBID) (Fig 2C and Appendix Fig S1D). Thus, although our data put forth a preferential link between E2F1 and BAK, this may be not exclusive and BAX may contribute under certain circumstances.

We then investigated whether the non-transcriptional pro-apoptotic impact of E2F1 on BCL-xL-regulated BAK-mediated MOMP relied on a molecular interaction between E2F1 and BCL-xL, which both localize at intracellular membranes and at the mitochondria in particular (Fig 1B and EV1A). As shown in figure 3A, E2F1 co-immunoprecipitated with BCL-xL in lysates from Saos-2 cells. Importantly, this interaction was detected in numerous other cell lines independently from their pRB and p53 status (Fig 3A and EV4A). Bioluminescence resonance energy transfer (BRET) assays confirmed a specific proximity between Renilla Luciferase fused to E2F1 (RLuc-E2F1) and YFP-BCL-xL at a whole cell level (Fig 3B). In sharp contrast to these observations, we could not detect any BRET signals between E2F1 and BAK by BRET experiments (Fig EV4B). Moreover, pull-down assays using recombinant GST fused E2F1 [25] and recombinant soluble BCL-xL demonstrated a direct interaction between both proteins (Fig 3C). We mapped the minimal domain required for E2F1 to interact with BCL-xL to the DNA Binding Domain: fusion proteins containing this region only (DBD, residues 114-191, Fig EV1B and Appendix Fig S1A) showed BRET signals with BCL-xL (Fig 3B) and pulled down recombinant BCL-xL (Fig 3C). E2F1 deleted in its C-terminal end (ΔC, Fig EV1B and Appendix Fig S1A) behaved similarly (Fig 3B) but a form deleted in its N-terminal end that encompasses the DBD (ΔN, Fig EV1B and Appendix Fig S1A) showed strongly reduced BRET signals and pull-down properties (Fig 3B and EV4C). Consistent with the notion that its interaction with BCL-xL contributes to E2F1

pro-apoptotic activity, and in agreement with preceding results [18], ectopic expression of the DBD and ΔC forms, but not of the ΔN one, induced cell death, MOMP and caspase activity (Fig 3D and EV4D).

Arguing for a BH3 binding site independent interaction between E2F1 and BCL-xL, E2F1/BCL-xL co-immunoprecipitations were unaffected by WEHI-539 treatment (Fig 3A). Moreover, BRET signals between E2F1 and BCL-xL were left intact by the R139D or G138E R139L I140N substitutions in BCL-xL, which significantly affected BRET signals between BAK and BCL-xL (Fig EV4E-F). Notably, recombinant E2F1 had no detectable effect when added to BAK-expressing isolated mitochondria, it did not enhance tBID induced cytochrome C release and it did not derepress BCL-xL inhibition of cytochrome C release under these conditions (J.C. Martinou, personal communications). E2F1 is thus unlikely to function as a competitive inhibitor of BCL-xL to prevent its inhibition of BAK, arguing that it indirectly interferes with BAK/BCL-xL physical and/or functional interactions, as was reported for the DNA binding Domain of p53 [26,27]. To investigate this further, we explored whether E2F1 would mitigate BCL-xL control over BAK by impacting on a dynamic process, only patent in whole cell assays. Changes in BCL-xL retrotranslocation have been suggested to impact on its anti-apoptotic function [28]. To directly investigate whether BCL-xL shuttling is critical for its ability to inhibit BAK mediated apoptosis, we compared the ability of two variants of BCL-xL (endowed with enhanced retrotranslocation properties) BCL-xL Δ2 and BCL-xL-T_{BAX} [28] to antagonize BAK-induced cell death with that of BCL-xL. These variants more efficiently prevented BAK-induced cell death, indicating that changes in BCL-xL localization dynamics impact on its control over BAK. Apoptosis suppression by BCL-xL required its mitochondrial localization since no protection was observed with the cytosolic BCL-xL A221R variant (Fig 4A and Appendix Fig S1E) [29]. Of note, BCL-xL Δ2 and BCL-xL-T_{BAX} were not detectably more efficient against BAX-induced cell death than wild type BCL-xL (Fig 4A). This could be due to the fact that BAX is intrinsically more mobile than BAK [12]. Alternatively, the cell death rates induced by BAX in these assays may be too low to detect improved protection when BCL-xL retrotranslocation is enhanced.

We then investigated the effects of E2F1 on the subcellular localization dynamics of BCL-xL. To this end, we used MCF-7 cells stably expressing YFP-BCL-xL and performed fluorescence recovery after photobleaching (FRAP) experiments as described in [13–15]. These cells were transiently transfected with mCherry fused to E2F1 forms (wt, OTC and E132), and we investigated YFP-BCL-xL mobility between the cytosol and mitochondria in red fluorescent cells. We controlled that YFP- fused BCL-xL interacted with wt or E132 forms under these circumstances (Fig EV5A). FRAP studies on cells expressing the negative control mCherry revealed that YFP-BCL-xL recovered to about 80% of its initial fluorescence (Fig 4B). This indicates that 4/5 of BCL-xL molecules are mobile and that only the 20% remainders are stably associated with the outer mitochondrial membrane. In cells over-expressing E2F1, YFP-BCL-xL only recovered to 60% of its initial fluorescence, indicating a two-fold increase (20% to 40%) of BCL-xL molecules stably associated to the outer mitochondrial membrane compared to controls. We observed the same decrease in recovery rates for the E132 or OTC forms (Fig 4B). Similar conclusions were drawn using mouse embryonic fibroblasts stably expressing GFP-BCL-xL (Fig EV5B). These experiments support the notion that E2F1, independently from transcription, stabilizes BCL-xL association with mitochondrial membranes, thereby limiting retrotranslocation rates required, as shown above, for full inhibition of BAK.

To the best of our knowledge, our work is the first one to describe how BCL-xL subcellular localization dynamics impact on its ability to inhibit cell death (mediated by BAK in particular), and to define one regulatory element thereof, namely E2F1. Inhibition of BCL-xL retrotranslocation (upon E2F1 accumulation or mutations in its C-terminal end) might erode its anti-apoptotic activity by precluding active shuttling of BCL-xL pro-apoptotic binding partners BAK, but also possibly BAX or BH3 activators, away from their site of oligomerization and action [13,15,28]. Alternatively, it might prevent interactions of BCL-xL with non-mitochondrial effectors, involved in its anti-apoptotic function. Interestingly, changes in BCL-xL shuttling also impact on the cell response to BH3 mimetics, since membrane localization of BCL-xL selectively influences its binding to the BH3 domains of apoptotic effectors [29]. Thus, modifications in the respective amounts of mobile versus mitochondrial-stable BCL-xL molecules are functionally relevant and they represent a critical level of regulation of BCL-xL survival function. We show here that these changes can be modulated independently from BCL-xL BH3 binding as E2F1 impacts on BCL-xL localization dynamics while interacting with it at a site that appears different from its BH3 binding one. The reported effect of E2F1 might extend to retrotranslocation of the other inhibitor of BAK, MCL-1 [30]. Of note, another implication of our work is that differences in BCL-xL localization dynamics may be found between cancer versus normal cells due to differences in E2F1 expression and activity [31]. In all cases, it underscores that the BCL-2 regulated apoptotic network has to be considered as a dynamically evolving one, which is influenced by tumor suppressor pathways not only at the level of synthesis rates and protein complex formation but also at the level of shuttling kinetics between subcellular membranes and the cytosol.

MATERIALS AND METHODS

Cell Culture and reagents

Cells lines were obtained from ATCC excepted the HCT116 $p21^{-/-}$ cell line that was kindly provided by Dr Volgenstein. Saos-2 and HCT116 p21-/- were cultured in Mc Coy's 5A; MCF-7 and BT-549 in $RPMI_{1640}$ and U251 in DMEM. MCF-7 stably overexpressing YFP-BCL-xL was obtained by transfection with peYFP-BCL-xL and selection with G418. MDA-MB-231 OMI-mCherry cells were selected with puromycine after infection with retroviruses (MOI 3) containing vector coding for human OMI sequence fused to the mCherry sequence. Cells with moderate expression of OMI-mCherry were sorted with the BD-FACS ARIA III sorter. All transfections were performed using Lipofectamine 2000 according to the manufacturer's instructions.
Unless indicated otherwise, treatments were used at the following concentrations: 2µM of Wehi-539 (ApexBio), 50µM of Etoposide (Sigma) and 5µM de Q-VD-OPh (R&D System).

Flow cytometry

Apoptosis analysis was evaluated by staining cells with Annexin V-APC (BD Pharmingen) or with anti-cleaved caspase3-AlexaFluor 647 antibody (9602, Cell Signaling) according to the manufacturer's instructions and performed on FACS Calibur (BD Biosciences) using the CellQuestPro software (Becton–Dickinson). MOMP quantification in MDA-MB231 OMI-mCherry cells was determined by evaluating the mCherry low fluorescence cell percentage using the BD-FACS ARIA III (BD-Biosciences) operated by the DIVA software.

Plasmids

The pcDNA3.1, peYFP-C1 and pRLuc-C1 plasmids were used to express BCL-2 family proteins. YFP-TM_{BCL-xL} contains the 209 to 233 amino acid of BCL-xL. BCL-xL Δ2 and BCL-xL-T_{BAX} alleles were kindly provided by F. Edlich. Human E2F1 and the ΔC, DBD and ΔN encoding sequences were cloned in peGFP-C1, pmCherry-C1, pRLuc-C1 or pGEX-4T1 plasmids to express the GFP, mCherry, RLuc and GST fusion E2F1 proteins, respectively. ΔC, DBD and ΔN sequences lead to the expression of E2F1 amino-acids residues 1-214, 114-191 and 191-437 respectively. The mitochondrial targeting sequence of ornithine

carbamoyltransferase (OTC) from Lwtp53 plasmid [6] was cloned in fusion with GFP- and mCherry-E2F1 encoding sequence. L132E N133F point mutations (E132 allele) were introduced by directed mutagenesis.

siRNAs and transfection

The following siRNAs were used: siE2F1 (HSC.RNAI.N005225.10.3), siBAX (ON-TARGETplus BAX siRNA smart pool L-003308-01), siBAK (ON-TARGETplus BAK1 siRNA smart pool L-003305-00), and SiControl (ON-TARGETplus Non-targeting pool D-001810-10-20). Plasmids and siRNAs were transfected according to manufacturer's instructions (Invitrogen) using Lipofectamine 2000 and Lipofectamine RNAi Max, respectively.

RNA Extraction, reverse Transcription and real-time quantitative qPCR

RNAs were extracted using Nucleospin® RNA (Macherey Nagel). Reverse transcription was performed using Maxima First Strand cDNA Synthesis Kit for qPCR (Thermo Scientific). qPCR was realized on Stratagene Mx3005P thermocycler (Agilent Technologies) using Maxima SYBR Green qPCR Master Mix (2X) ROX kit (Thermo Scientific).

The following couple of primers were used for qPCR analysis:

TP73: 5'- CTTCAACGAAGGACAGTCTG / AAGTTGTACAGGATGGTGGT-3'
BBC3: 5'- ACCTCAACGCACAGTACGA / GCACCTAATTGGGCTCCATC-3'
BCL2L11: 5'- GCCTTCAACCACTATCTCAG / TAAGCGTTAAACTCGTCTCC-3'
HRK: 5'- CAGGCGGAACTTGTAGGAAC / AGGACACAGGGTTTTCACCA-3'

Immunoblot analysis and antibodies

Proteins were obtained by lysing cells with CHIP buffer (SDS 1%, EDTA 10nM, Tris-HCl [pH 8,1] 50nM and proteases/phosphatases inhibitor Pierce) followed by sonication prior separation on SDS-PAGE.

The following antibodies were used: ACTIN (MAB1501R) and BIM (AB17003) from Millipore, E2F1 (3742), COXIV (4850), PUMA (4976), BID (2002S) and BAK (3814) from Cell Signaling, BAX (A3533) and BCL-2 (M0887) from Dako, BCL-xL ([E18] Ab32370) and GFP (Ab290) from Abcam, MCL-1 (sc-819), LAMIN A/C (sc-376248) and KTN (sc-33562) from Santa Cruz, PARP (#AM30) from Calbiochem. Clarity™ western ECL kit (Biorad) was used for Immunoblot revelation.

Heavy membrane fractionation and mitochondria purification

MCF7 and HeLa heavy membranes fraction were prepared by differential centrifugations as described in detail previously [32]. Saos2 subcellular fractionation to isolate heavy membranes fraction was performed using Mitochondria Isolation Kit for Cultured Cells (Thermo Scientific) based on differential centrifugations. Briefly, cells were lysed in the supplied buffer with proteases/phosphatases inhibitor by using a dounce homogenizer. Sequential centrifugation (3x700g 10 min and 12000g 20 min) leads to pellet the heavy membrane fraction. Pellet was resuspended with CHIP buffer and was used for Western blot analysis. A subcellular fraction enriched in intact mitochondria was prepared from Saos2 cells using the MACS Technology and superparamagnetic microbeads conjugated to anti-TOM22 antibody (Mitochondria isolation kit, Miltenyi Biotec). Briefly, cells were homogenized in the supplied lysis buffer by using a dounce homogenizer. Lysate was incubated with anti-TOM22 magnetic beads for 1 hour at 4°C before magnetically separating the mitochondria on the MACS column. The magnetically labeled mitochondria were resuspended with CHIP buffer and was used for Western blot analysis. Total extract was obtained by directly lysing cells in CHIP buffer.

Immunoprecipitation assay

Protein lysates were obtained by lysing cells with PBS-1%CHAPS buffer containing proteases/phosphatases inhibitor and clarification at 13 000g 15 min 4°C. Immunoprecipitation was performed on 500μg of protein lysates incubated with 10μl of anti-BCL-xL or anti-E2F1 antibodies by using the PureProteome™ Protein G Magnetic Beads protocol (Millipore).

Pull-down assay

Recombinant proteins: GST, GST-E2F1, GST-ΔC, GST-DBD and GST-ΔN were produced in *E. Coli,* prior immobilization on glutathion-sepharose (Amersham Biosciences), followed by incubation with 100ng of recombinant BCL-xL (Biorbyt). Interactions were evaluated by immunoblotting anti-BCL-xL ([E18] Ab32370) or anti-GST (Rockland).

BRET saturation curves assays

BRET experiments were performed as described in [29]. Briefly, cells were plated in 12-well plates and transfected with increasing amounts (50 to 1500 ng/well) of plasmids coding for a BRET acceptor (YFP-BCL-

xL, YFP-BCL-xL R139D, YFP-BCL-xL G138E R139L I140N, YFP-$TM_{BCL\text{-}xL}$ or YFP-BAK), and constant amounts (50 ng/well) of plasmid expressing a BRET donor (RLuc-E2F1, RLuc-ΔC, RLuc-ΔN, RLuc-BAK and RLuc-BCL-xL). BRET measurement was performed using the lumino/fluorometer Mithras LB 940 (Berthold Technologies, France) after addition of Coelenterazine H substrate (Interchim) (5 µM). BRET signal corresponds to the emission signal values (530 nm) divided by the emission signal values (485 nm). The BRET ratio was calculated by subtracting the BRET signal value obtained with co-expressed donor and acceptor by that obtained with the donor protein co-expressed with untagged BCL-xL. Data shown are representative of at least three independent experiments.

Microscopy and FRAP assay
MOMP imaging was performed using HCS Array Scan Thermo. Prior fluorescence images of Saos-2, cells were incubated with 100nM Mitotracker Red CMXRos (Life Technologies, M7512) and 1μg/mL Hoescht, 20 min 37°C. Acquisition was realized using Zeiss Axio Observer Z1. Live imaging was performed on a Zeiss Axio Observer Z1 with a CSU-X1 spinning disk (Yokogawa), using a 63×/1.40 Plan Apo lens, an Evolve EMCCD camera (Photometrics), and a motorized XYZ stage (Applied Scientific Instrumentation) driven by Marianas hardware and SlideBook 5.0 software (Intelligent Imaging Innovations). FRAP implies one region reach in BCL-xL fluorescence was bleached (one iteration, 488nm, 100%, 10ms) and images were captured every 5 sec. FIJI software was used for analysis. Fluorescence background was substracted, prior quantifying fluorescence of the FRAP region using ROI manager pluging in FIJI. Data were normalized to 100% fluorescence prebleaching. Statistical analysis was calculated using non-linear regression analysis in GraphPad Prism 5.0.

Statistical Analysis
Unpaired student's *t* test was used for statistical analysis with GraphPad Prism 5.0 Software. Errors bars represent standard errors of mean (SEM). The symbols correspond to a P-value inferior to *0.05, **0.01, ***0.001 and **** 0.0001.

ACKNOWLEDGEMENTS

We thank members of the "Stress Adaptation and Tumor Escape" laboratory for their technical advice, fruitful comments and enthusiasm. We thank S. Tait for the generous gift of the OMI-Cherry retroviral vector, F. Edlich for the BCL-xL Δ2 and BCL-xL-T_{BAX} constructs and U. Moll for the Lwtp53 plasmid. We are grateful for technical support from the Cellular and Tissular Imaging (MicroPICell), from the Molecular Interactions and Protein Activities (IMPACT) and from Cytometry (CytoCell) Core Facilities of Nantes University. We thank S. Montessuit and J.C. Martinou for cytochrome C release assay on isolated mitochondria. CV, SL, and LK are supported by fellowships from the Ministère de la Recherche et de l'Enseignement Supérieur, Ligue contre le cancer 44 and by a MCRC-CRUK training award, respectively. The Wellcome Centre for Cell-Matrix Research is supported by Wellcome Trust. This work was supported by Région Pays de la Loire (CIMATH2), Ligue contre le Cancer (R13137), ARC (R15083NN), and INCA PLBio 2013 (R12134NN).

AUTHOR CONTRIBUTIONS

CV, SL, AF, JA, CK, LE, and FB conducted experiments and analyzed the data. CV, SBN, FG, LD, APG, PPJ and LM designed the experiments and interpreted results. PPJ and LM conceived the study, supervised it and wrote the manuscript.

CONFLICT OF INTEREST

The authors declare that they have no conflict of interest.

REFERENCES

1. Polager S, Ginsberg D (2009) p53 and E2f: partners in life and death. *Nat Rev Cancer* **9**: 738–748.
2. Chipuk JE, Fisher JC, Dillon CP, Kriwacki RW, Kuwana T, Green DR (2008) Mechanism of apoptosis induction by inhibition of the anti-apoptotic BCL-2 proteins. *Proc Natl Acad Sci U S A* **105**: 20327–20332.
3. Martinou J-C, Youle RJ (2011) Mitochondria in apoptosis: Bcl-2 family members and mitochondrial dynamics. *Dev Cell* **21**: 92–101.
4. Tait SWG, Green DR (2010) Cell survival in tough times: The mitochondrial recovery plan. *Cell Cycle Georget Tex* **9**: 4254–4255.
5. Juin P, Geneste O, Gautier F, Depil S, Campone M (2013) Decoding and unlocking the BCL-2 dependency of cancer cells. *Nat Rev Cancer* **13**: 455–465.
6. Marchenko ND, Zaika A, Moll UM (2000) Death signal-induced localization of p53 protein to mitochondria. A potential role in apoptotic signaling. *J Biol Chem* **275**: 16202–16212.
7. Mihara M, Erster S, Zaika A, Petrenko O, Chittenden T, Pancoska P, Moll UM (2003) p53 has a direct apoptogenic role at the mitochondria. *Mol Cell* **11**: 577–590.
8. Chipuk JE, Kuwana T, Bouchier-Hayes L, Droin NM, Newmeyer DD, Schuler M, Green DR (2004) Direct activation of Bax by p53 mediates mitochondrial membrane permeabilization and apoptosis. *Science* **303**: 1010–1014.
9. Le Pen J, Laurent M, Sarosiek K, Vuillier C, Gautier F, Montessuit S, Martinou JC, Letaï A, Braun F, Juin PP (2016) Constitutive p53 heightens mitochondrial apoptotic priming and favors cell death induction by BH3 mimetic inhibitors of BCL-xL. *Cell Death Dis* **7**: e2083.
10. Lindsay J, Esposti MD, Gilmore AP (2011) Bcl-2 proteins and mitochondria--specificity in membrane targeting for death. *Biochim Biophys Acta* **1813**: 532–539.
11. Montero J, Sarosiek KA, DeAngelo JD, Maertens O, Ryan J, Ercan D, Piao H, Horowitz NS, Berkowitz RS, Matulonis U, et al. (2015) Drug-induced death signaling strategy rapidly predicts cancer response to chemotherapy. *Cell* **160**: 977–989.
12. Todt F, Cakir Z, Reichenbach F, Emschermann F, Lauterwasser J, Kaiser A, Ichim G, Tait SWG, Frank S, Langer HF, et al. (2015) Differential retrotranslocation of mitochondrial Bax and Bak. *EMBO J* **34**: 67–80.
13. Edlich F, Banerjee S, Suzuki M, Cleland MM, Arnoult D, Wang C, Neutzner A, Tjandra N, Youle RJ (2011) Bcl-x(L) retrotranslocates Bax from the mitochondria into the cytosol. *Cell* **145**: 104–116.
14. Lauterwasser J, Todt F, Zerbes RM, Nguyen TN, Craigen W, Lazarou M, van der Laan M, Edlich F (2016) The porin VDAC2 is the mitochondrial platform for Bax retrotranslocation. *Sci Rep* **6**: 32994.
15. Schellenberg B, Wang P, Keeble JA, Rodriguez-Enriquez R, Walker S, Owens TW, Foster F, Tanianis-Hughes J, Brennan K, Streuli CH, et al. (2013) Bax exists in a dynamic equilibrium between the cytosol and mitochondria to control apoptotic priming. *Mol Cell* **49**: 959–971.
16. Bertin-Ciftci J, Barré B, Le Pen J, Maillet L, Couriaud C, Juin P, Braun F (2013) pRb/E2F-1-mediated caspase-dependent induction of Noxa amplifies the apoptotic effects of the Bcl-2/Bcl-xL inhibitor ABT-737. *Cell Death Differ* **20**: 755–764.
17. Poppy Roworth A, Ghari F, La Thangue NB (2015) To live or let die - complexity within the E2F1 pathway. *Mol Cell Oncol* **2**: e970480.
18. Hsieh JK, Fredersdorf S, Kouzarides T, Martin K, Lu X (1997) E2F1-induced apoptosis requires DNA binding but not transactivation and is inhibited by the retinoblastoma protein through direct interaction. *Genes Dev* **11**: 1840–1852.
19. Phillips AC, Bates S, Ryan KM, Helin K, Vousden KH (1997) Induction of DNA synthesis and apoptosis are separable functions of E2F-1. *Genes Dev* **11**: 1853–1863.
20. Hilgendorf KI, Leshchiner ES, Nedelcu S, Maynard MA, Calo E, Ianari A, Walensky LD, Lees JA (2013) The retinoblastoma protein induces apoptosis directly at the mitochondria. *Genes Dev* **27**: 1003–1015.
21. Tait SWG, Parsons MJ, Llambi F, Bouchier-Hayes L, Connell S, Muñoz-Pinedo C, Green DR (2010) Resistance to caspase-independent cell death requires persistence of intact mitochondria. *Dev Cell* **18**: 802–813.
22. Hao H, Chen C, Rao X-M, Gomez-Gutierrez JG, Zhou HS, McMasters KM (2012) E2F-1- and E2Ftr-mediated apoptosis: the role of DREAM and HRK. *J Cell Mol Med* **16**: 605–615.
23. Bell LA, O'Prey J, Ryan KM (2006) DNA-binding independent cell death from a minimal proapoptotic region of E2F-1. *Oncogene* **25**: 5656–5663.
24. Ding J, Mooers BHM, Zhang Z, Kale J, Falcone D, McNichol J, Huang B, Zhang XC, Xing C, Andrews DW, et al. (2014) After embedding in membranes antiapoptotic Bcl-XL protein binds both Bcl-2 homology region 3 and helix 1 of proapoptotic Bax protein to inhibit apoptotic mitochondrial permeabilization. *J Biol Chem* **289**: 11873–11896.

25. Cartier J, Berthelet J, Marivin A, Gemble S, Edmond V, Plenchette S, Lagrange B, Hammann A, Dupoux A, Delva L, et al. (2011) Cellular inhibitor of apoptosis protein-1 (cIAP1) can regulate E2F1 transcription factor-mediated control of cyclin transcription. *J Biol Chem* **286**: 26406–26417.
26. Hagn F, Klein C, Demmer O, Marchenko N, Vaseva A, Moll UM, Kessler H (2010) BclxL changes conformation upon binding to wild-type but not mutant p53 DNA binding domain. *J Biol Chem* **285**: 3439–3450.
27. Han J, Goldstein LA, Hou W, Gastman BR, Rabinowich H (2010) Regulation of mitochondrial apoptotic events by p53-mediated disruption of complexes between antiapoptotic Bcl-2 members and Bim. *J Biol Chem* **285**: 22473–22483.
28. Todt F, Cakir Z, Reichenbach F, Youle RJ, Edlich F (2013) The C-terminal helix of Bcl-x(L) mediates Bax retrotranslocation from the mitochondria. *Cell Death Differ* **20**: 333–342.
29. Pécot J, Maillet L, Le Pen J, Vuillier C, Trécesson S de C, Fétiveau A, Sarosiek KA, Bock FJ, Braun F, Letai A, et al. (2016) Tight Sequestration of BH3 Proteins by BCL-xL at Subcellular Membranes Contributes to Apoptotic Resistance. *Cell Rep* **17**: 3347–3358.
30. Xu S, Peng G, Wang Y, Fang S, Karbowski M (2011) The AAA-ATPase p97 is essential for outer mitochondrial membrane protein turnover. *Mol Biol Cell* **22**: 291–300.
31. Hsu Y-T, Wolter KG, Youle RJ (1997) Cytosol-to-membrane redistribution of Bax and Bcl-XL during apoptosis. *Proc Natl Acad Sci U S A* **94**: 3668–3672.
32. Gautier F, Guillemin Y, Cartron PF, Gallenne T, Cauquil N, Le Diguarher T, Casara P, Vallette FM, Manon S, Hickman JA, et al. (2011) Bax Activation by Engagement with, Then Release from, the BH3 Binding Site of Bcl-xL. *Mol Cell Biol* **31**: 832–844.

FIGURE LEGENDS

Figure 1. E2F1 localizes to mitochondria in Saos-2 cells, where it promotes apoptosis

(A) Apoptotic signal induces E2F1 stabilization. Saos-2 cells were treated for 16h by 50 μM etoposide or not (untreated) before western-blot analysis of E2F1 expression and PARP1 cleavage. (B) Etoposide induces apoptosis in E2F1 dependent manner. Saos-2 cells were transfected with control or E2F1 siRNA for 24h and treated as in (A) before cell death analysis by trypan blue staining. Western blot controlling the E2F1 siRNA extinction is inserted. (C) E2F1 constitutively localizes to mitochondria. Saos-2 cells were fractionated and equal amounts of total lysate versus heavy membrane fraction (HM fraction) or mitochondria enriched fraction (Mito fraction) were analyzed by Western blot analysis for E2F1 and BCL-xL expression. KTN, LAMIN A/C and COX IV serve as markers of endoplasmic reticulum, nuclei and mitochondria respectively. Data shown are representative of at least three independent experiments. (D) Ectopic E2F1 expression triggers apoptosis. Saos-2 cells were transfected with the indicated E2F1 expression vectors and treated or not with etoposide (50 μM) for an additional 48h. Apoptosis was evaluated by Annexin V-APC staining among GFP positives cells using flow cytometry analysis. (E) E2F1 triggers MOMP. MDA-MB231 cells stably expressing OMI-mCherry were transfected with the indicated expression vectors. 48 h post-transfection, MOMP was quantified by determining the mCherry low fluorescence cell percentage among GFP positive cells using flow cytometry analysis.

Data information: *P<0.05, **P<0.01, ***P<0.001, ****P<0.0001 versus control (Student's t-test). Graph bars represent the average of at least three independent experiences and the error bars show the S.E.M. Source data are available online for this figure.

Figure 2. E2F1 promotes mitochondrial apoptosis controlled by the BCL-2 family

(A) E2F1 induced apoptosis in a BAK dependent manner. Saos-2 cells were transfected with control, BAK or BAX siRNAs. 24h later, cells were transfected with the expression vectors coding for either GFP-E2F1, or OTC-GFP-E2F1 for 48h before apoptosis measurement as described in figure 1D. (B) BCL-xL suppresses E2F1-induced apoptosis as a BH3-binding protein. Saos-2 cells were co-transfected with plasmids encoding the indicated anti-apoptotic proteins (BCL-xL or its R139D mutant, BCL-2 or MCL-1) and GFP, GFP-E2F1 or OTC-GFP-E2F1 in a molecular ratio 3:1. 24h later, apoptosis was analyzed as described in figure 1D. (C) Mitochondria-targeted E2F1 promotes cell death activity induced by BAK, BAX or BH3-only activators overexpression. Saos-2 cells were co-transfected with the indicated expression vectors and for GFP, GFP-E2F1 or OTC-GFP-E2F1 in a molecular ratio 3:1. 24h later, apoptosis was analyzed as described in figure 1D. The deficient activator PUMA 3A, carrying L141A D146A L148A substitutions in the BH3 domain was used as a negative control.

Data information: *P<0.05, **P<0.01, ***P<0.001, ****P<0.0001 versus control (Student's t-test). Graph bars represent the average of at least three independent experiences and the error bars show the S.E.M.

Figure 3. E2F1 interacts with BCL-xL

(A) E2F1 interacts with BCL-xl in a BH3-mimetic resistant manner. Endogenous BCL-xL was immune-precipitated from Saos-2 cells extracts treated or not with WEHI-539 (1 μM for 24h) with anti-BCL-xL or negative control anti-GFP, then endogenous E2F1 association was assessed by Western blotting. (B) E2F1 and BCL-xL interact in live cells. BRET saturation assay analysis was performed in MCF-7 cells using

increasing amount of vectors encoding for YFP-BCL-xL or YFP-TM-$_{BCL-xL}$ in the presence of a fixed amount of the vector encoding RLuc-E2F1, RLuc-ΔC, RLuc-DBD or RLuc-ΔN. BRET ratios are measured for every YFP-BCL-xL plasmid concentrations and are plotted as a function of the ratio of total acceptor fluorescence to donor luminescence. No BRET saturation curve was obtained either using RLuc-E2F1 and YFP fused to the C-terminal transmembrane domain of BCL-xL (YFP-TM$_{BCL-xL}$) demonstrating the specific interaction between E2F1 and BCL-xL, either using RLuc-ΔN indicating that N-terminal domain of E2F1 is required to interact with BCL-xL. The data were fitted using a nonlinear regression equation assuming a single binding site. Data are representative of at least three independent experiments. (C) E2F1 DNA-binding domain interacts with BCL-xL as recombinant proteins. GST pull-down analysis was performed using recombinant GST-E2F1, GST-ΔC, GST-DBD and purified BCL-xL proteins. (D) E2F1 DNA-binding domain is sufficient to induce mitochondrial apoptosis. Saos-2 and MDA-MB231 expressing OMI-mCherry cells were transfected with the indicated expression vectors. 48 h later, apoptosis (left panel) and MOMP among GFP positives cells (right panel) were analyzed as described in figures 1D and 1E.

Data information: ***P<0.001, ****P<0.0001 versus control (Student's t-test). Graph bars represent the average of at least three independent experiences and the error bars show the S.E.M. Source data are available online for this figure.

Figure 4. BCL-xL mobility is decreased by E2F1 overexpression and it determines BAK-inhibition efficiency

(A) BCL-xL variants that enhanced its mobility (BCL-xL Δ2 and BCL-xL-T$_{BAX}$) inhibit BAK-mediated cell death more efficiently compared to BCL-xL. Saos-2 cells were co-transfected with plasmids encoding for the indicated BCL-xL variants together with YFP-BAK or YFP-BAX in a molecular ratio 3:1. 48 h later, apoptosis was analyzed as described in figure 1D. (B) E2F1 stabilizes BCL-xL on mitochondria. MCF-7 stably expressing YFP-BCL-xL, transfected with the expression vectors coding for either mCherry, mCherry-E2F1, OTC-mCherrry-E2F1 or mCherry-E132. 16 h post-transfection, cells were photobleached in the yellow region of interest (ROI) and imaged every 5s (prebleaching and 5, 50, 100, 150s after photobleaching are shown). Scale bar = 10 μm. Fluorescence intensity was analysed within the ROI and normalized to 100% (corresponding to fluorescence intensity before photobleaching) as shown in corresponding curves. Graph bars presented in the histogram showed the maximal percentage of fluorescence recovered after the photobleaching as determined by the fitting using a one phase exponential equation. Data presented are means of four independent experiments, corresponding to measure in at least 30 cells analyzed per condition.

Data information: *P<0.05, **P<0.01, ***P<0.001, ****P<0.0001 versus control (Student's t-test). Graph bars represent the average of at least three independent experiences and the error bars show the S.E.M.

EXPANDED VIEW FIGURE LEGENDS

Figure EV1. Related to Figure 1

(A) A fraction of E2F1 constitutively localizes to heavy membranes fraction in HeLa and MCF-7 cell lines. One of three representative western blot analysis of E2F1 and BCL-xL localization in heavy membrane and cytosol fractions of HeLa and MCF-7 cells (equal amount in micrograms of proteins). KTN, LAMIN A/C and COX IV served as markers of endoplasmic reticulum, nuclei and mitochondria respectively. Graph bars represent quantification of the relative ratio of LAMIN A/C or E2F1 protein in Heavy Membrane (HM) Fraction compared to Total Fraction. (B) Schematic of GFP-E2F1 constructs. GFP moiety was fused to the N-terminus of E2F1 in phase with the initiation codon. GFP-E132 has L132E and N133F substitutions within the DNA binding domain that abrogate DNA binding and transcriptional activity. Mitochondrial targeting was achieved by fusing the prototypical mitochondrial import leader of ornithin transcarbamoyltransferase (OTC) to the N terminus of GFP-E2F1 (OTC-GFP-E2F1). ΔC, DBD and ΔN domains correspond to amino-acid residues 1-214, 114-191 and 191-437 respectively. (C) Subcellular localization of GFP and OTC-GFP E2F1. Representative fluorescence microscopy image of Saos-2 cells transfected with the expression vectors coding either for GFP-E2F1 or OTC-GFP-E2F1 (green) are shown. Mitochondria were visualized using MitoTracker Red CMXRos probe (red). Scale bar = 10 μm. (D) Mitochondrial targeted, transcription deficient, E2F1 E132 induce apoptosis, while GFP mitochondrial targeting with the OTC sequence does not it. Saos-2 cells were transfected with expression vectors coding either for GFP, OTC-GFP-E132 or OTC-GFP. 48h post-transfection, apoptosis was evaluated by flow cytometry for Annexin V-APC stained cells among GFP-positive ones.

Data information: ***P<0.001 versus control (Student's t-test). Graph bars represent the average of at least three independent experiences and the error bars show the S.E.M. Source data are available online for this figure.

Figure EV2. Related to Figure 1

(A) E2F1 triggers caspase-3 activation. Flow cytometry analysis of cells transiently expressing GFP-E2F1 or OTC-GFP-E2F1 and stained using anti-active caspase-3-Alexa 647 antibody. (B) Caspase inhibition protects cells from GFP-E2F1 and OTC-GFP-E2F1 induced apoptosis. Saos-2 cells were transfected with expression vectors for either GFP-E2F1 or OTC-GFP-E2F1 and treated or not with the pan-caspase inhibitor Q-VD-OPh (5 μM) for 48h. Apoptosis was evaluated as described in figure EV1D. (C) Visualization of E2F1-induced MOMP. MDA-MB231 cells expressing OMI-mCherry and transfected with the indicated expression vectors were imaged with ArrayScan High-Content Systems. Representative fluorescence microscopy images are shown. Arrows denote GFP transfected cells undergoing MOMP. Scale bar = 10 μm. (D) Representative flow cytometry analysis of OMI-mCherry expressing MDA-MB231 cells among GFP (or GFP-E2F1) positive cells. (E) Apoptotic rates in MDA-MB231 determined by flow cytometry analysis as described above. (F) Mitochondrial targeting of OTC-GFP-E2F1 lacks transcriptional activity. E2F1 transcriptional activities of Saos-2 cells transfected with expression vectors for either GFP, GFP-E2F1, mitochondrial targeted OTC-GFP-E2F1 or transcription-deficient GFP-E132, were evaluated by RT-qPCR for E2F1 transcription target

genes (p73, BBC3, BCL2L11, HRK coding for TP73, PUMA, BIM and HARAKIRI proteins respectively). Results are depicted as normalized levels of interest mRNA compared to 3 housekeeping genes used as reference point.

Data information: *P<0.05, **P<0.01, ***P<0.001 versus control (Student's t-test). Graph bars represent the average of at least three independent experiences and the error bars show the S.E.M.

Figure EV3. Related to Figure 2

Transcription deficient E2F1 E132 acts synergistically with BAK or BH3-only activator to induce apoptosis. Saos-2 cells were co-transfected with expression vectors for either BAK or BH3-only activator and GFP or GFP-E132 in a molecular ratio 3:1. 24h later, apoptosis was evaluated as described in figure EV1D.

Data information: ***P<0.001, ****P<0.0001 versus control (Student's t-test). Graph bars represent the average of at least three independent experiences and the error bars show the S.E.M. Source data are available online for this figure.

Figure EV4. Related to Figure 3

(A) E2F1-BCL-xL interaction in different cell lines. Endogenous E2F1 was immune-precipitated with anti-E2F1 antibody or irrelevant rabbit IgG in MCF-7, U251, HCT116 p21-/-, BT549 and HeLa cells before immunoblot analysis E2F1 and BCL-xL. (B) BRET saturation curves between RLuc-BCL-xL and YFP-BAK (performed as described in figure 3B) validates the YFP-BAK as a BRET acceptor. Neither BRET signals was detected between RLuc-E2F1 and YFP-BAK. Data are representative of at least three independent experiments. (C) The C terminal domain of E2F1 does not interact with BCL-xL. GST pull-down analysis was performed using recombinant GST-E2F1, GST-ΔC, GST-DBD, GST-ΔN and purified BCL-xL proteins. (D) The E2F1 DNA-binding domain triggers caspase-3 activation. Flow cytometry analysis of cells transiently expressing GFP-ΔC, GFP-DBD or GFP-ΔN and stained using anti-active caspase-3-Alexa 647 antibody. (E) BRET saturation curves between RLuc-E2F1 and YFP-BCL-xL R139D or YFP-BCL-xL G138E R139L I140N were performed as described in figure 3B. RLuc-E2F1 and YFP fused to the C-terminal transmembrane domain of BCL-xL (YFP-$TM_{BCL\text{-}xL}$) were used as a negative control. (F) BRET saturation curves between RLuc-BAK and YFP-BCL-xL, YFP-BCL-xL R139D or YFP-BCL-xL G138E R139L I140N in MCF-7 cells were performed as described in figure 3B. RLuc-BAK and YFP fused to the C-terminal transmembrane domain of BCL-xL (YFP-$TM_{BCL\text{-}xL}$) were used as a negative control. Data are representative of at least three independent experiments.

Data information: *P<0.05, ***P<0.001 versus control (Student's t-test). Graph bars represent the average of at least three independent experiences and the error bars show the S.E.M. Source data are available online for this figure.

Figure EV5. Related to Figure 4

(A) YFP-BCL-xL co-immunoprecipitates with E2F1. MCF-7 stably expressing YFP-BCL-xL were transfected with vectors encoding FLAG-E2F1 or E2F1 E132 mutant, before lysis and immunoprecipitation with an anti-GFP antibody and western-blot analysis with E2F1 and BCL-xL antibodies. (B) FRAP analysis of BCL-xL in MEFs cells. MEFs stably expressing GFP-BCL-xL were transfected with expression vectors for either mCherry or mCherry-E2F1. 16 post-transfection, FRAP analysis was carried out as in figure 4B. Data

presented are means ± S.E.M of four independent experiments, corresponding to measure in at least 10 cells analyzed per condition. Scale bar = 10 μm.

Data information: **P<0.01 versus control (Student's t-test). Graph bars represent the average of at least three independent experiences and the error bars show the S.E.M. Source data are available online for this figure.

Figure 1

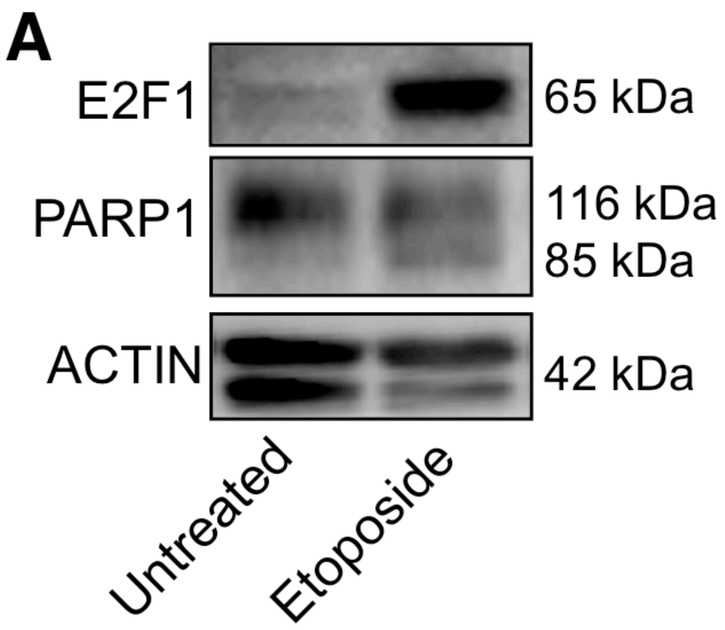
A
E2F1
65 kDa
PARP1
116 kDa
85 kDa
ACTIN
42 kDa
Untreated
Etoposide

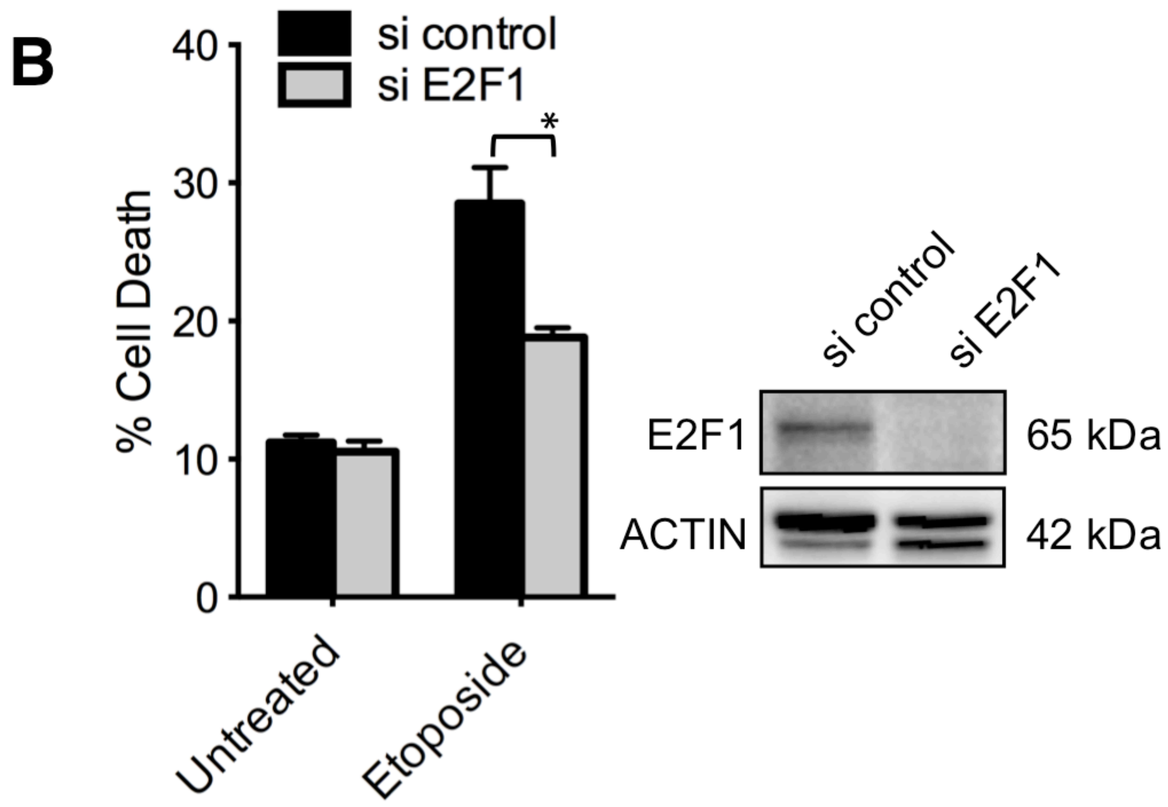
B
si control
si E2F1
% Cell Death
40
30
20
10
0
*
Untreated
Etoposide
si control
si E2F1
E2F1
65 kDa
ACTIN
42 kDa

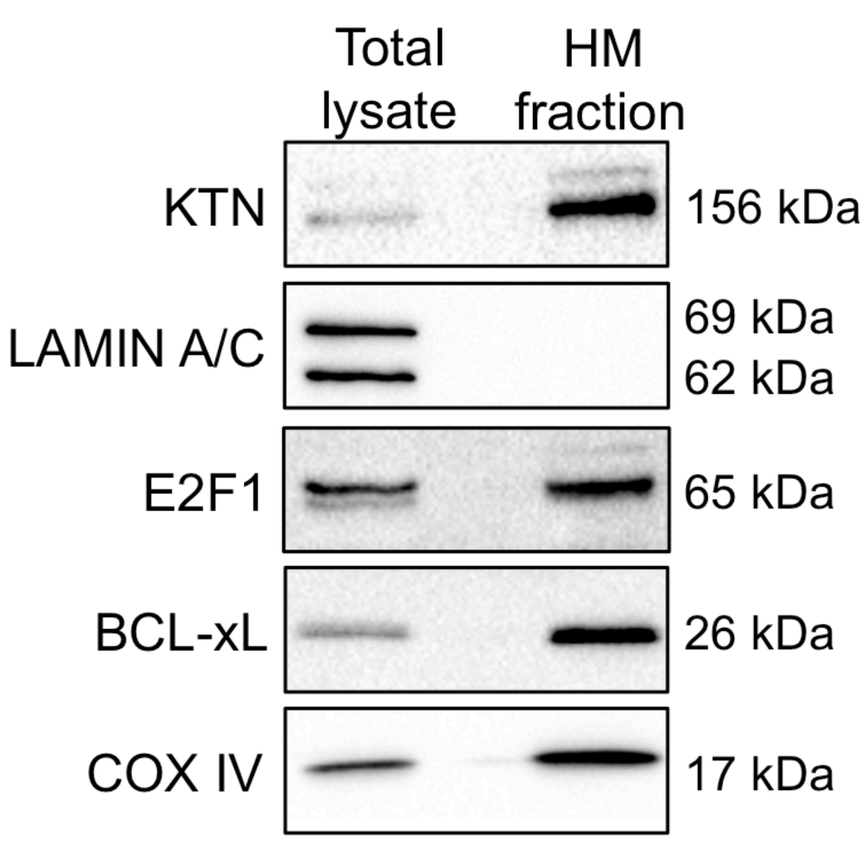
C
Total lysate
HM fraction
KTN
156 kDa
LAMIN A/C
69 kDa
62 kDa
E2F1
65 kDa
BCL-xL
26 kDa
COX IV
17 kDa

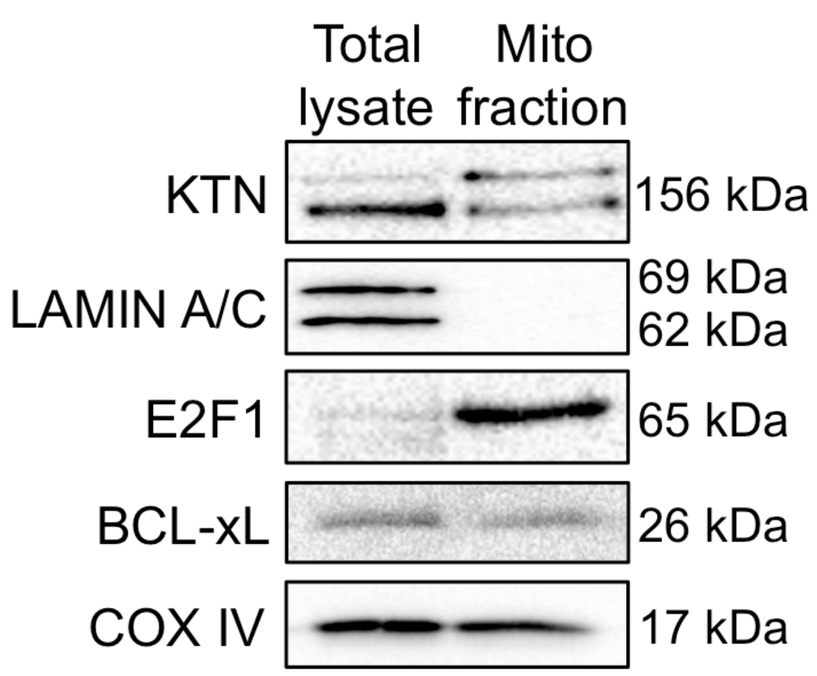
Total lysate
Mito fraction
KTN
156 kDa
LAMIN A/C
69 kDa
62 kDa
E2F1
65 kDa
BCL-xL
26 kDa
COX IV
17 kDa

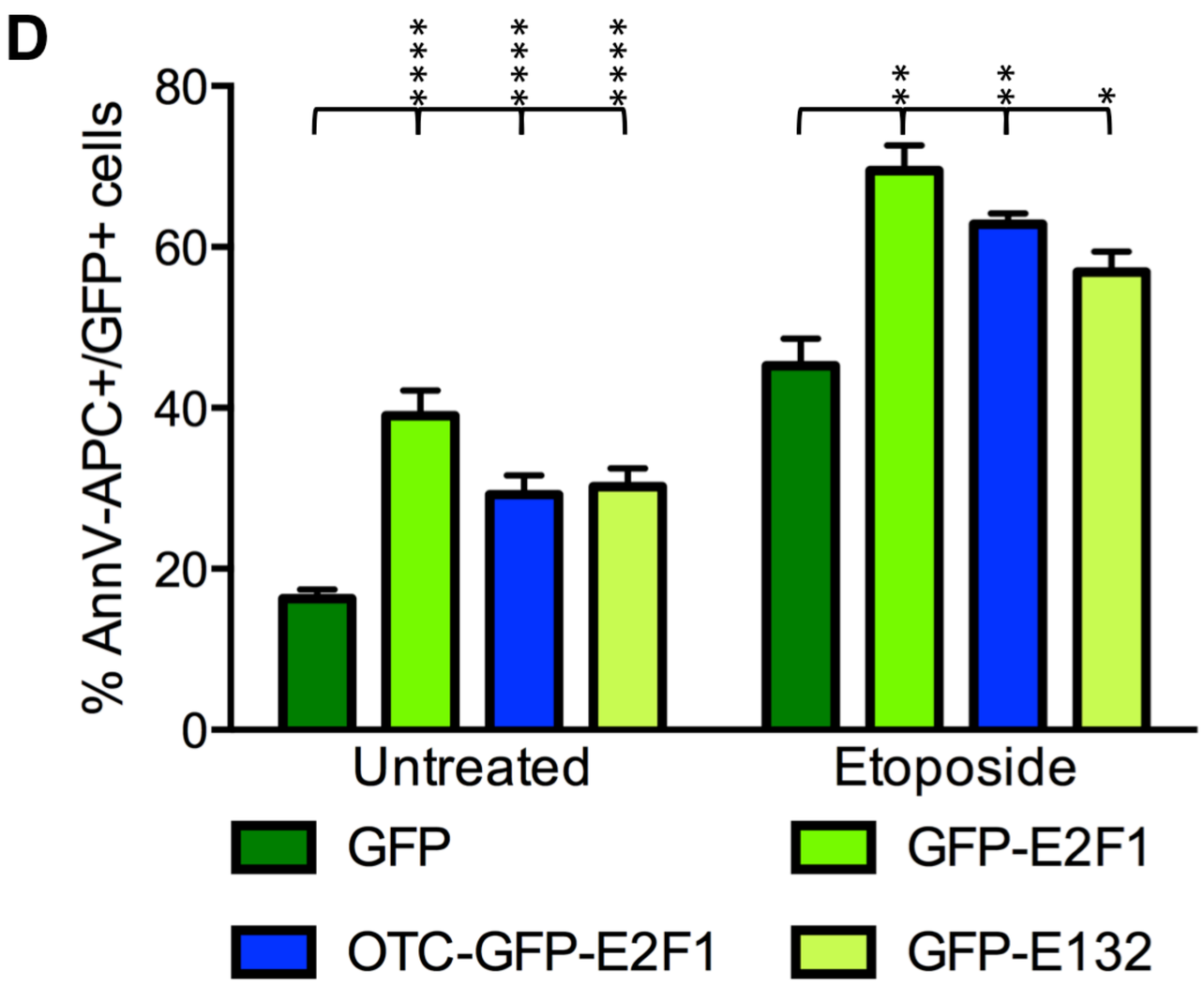
D
% AnnV-APC+/GFP+ cells
80
60
40
20
0
Untreated
Etoposide
GFP
GFP-E2F1
OTC-GFP-E2F1
GFP-E132

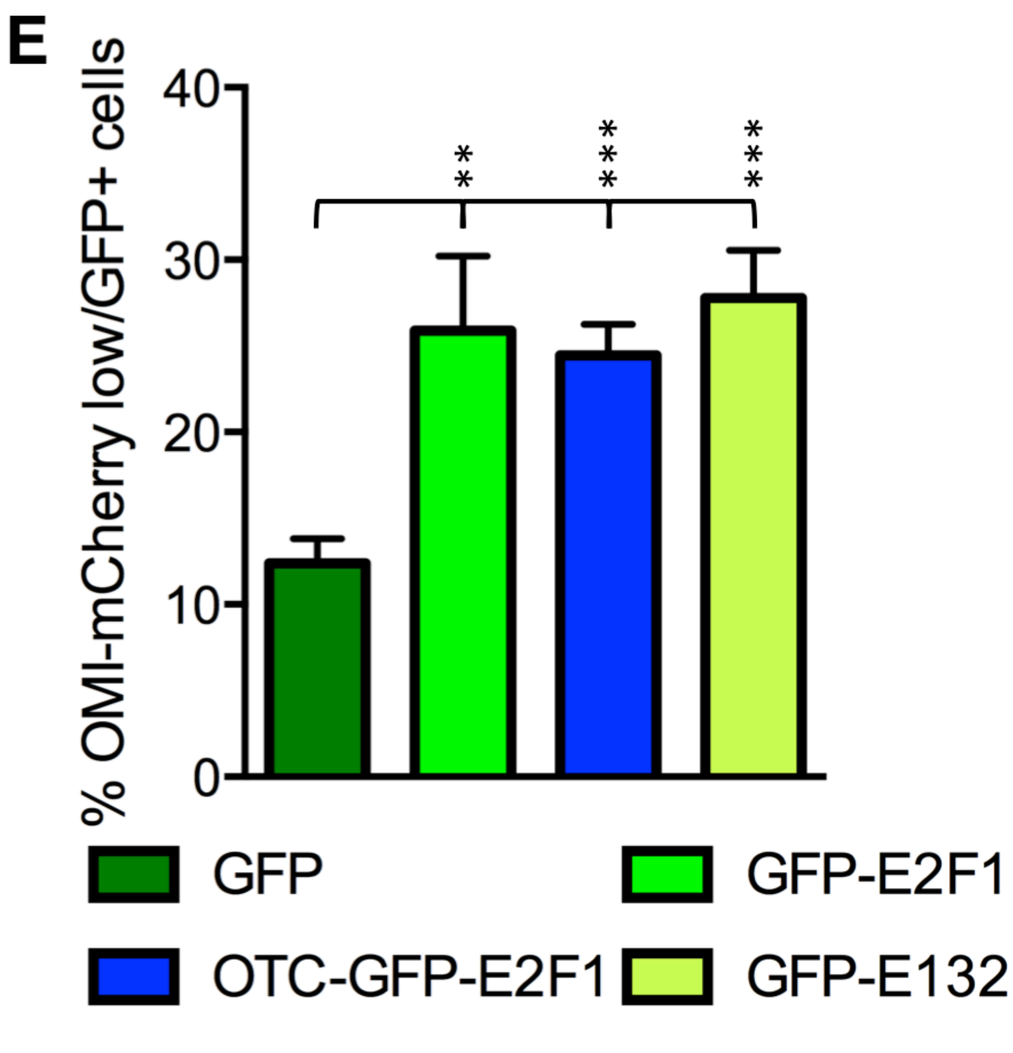
E
% OMI-mCherry low/GFP+ cells
40
30
20
10
0
GFP
GFP-E2F1
OTC-GFP-E2F1
GFP-E132

Figure 2

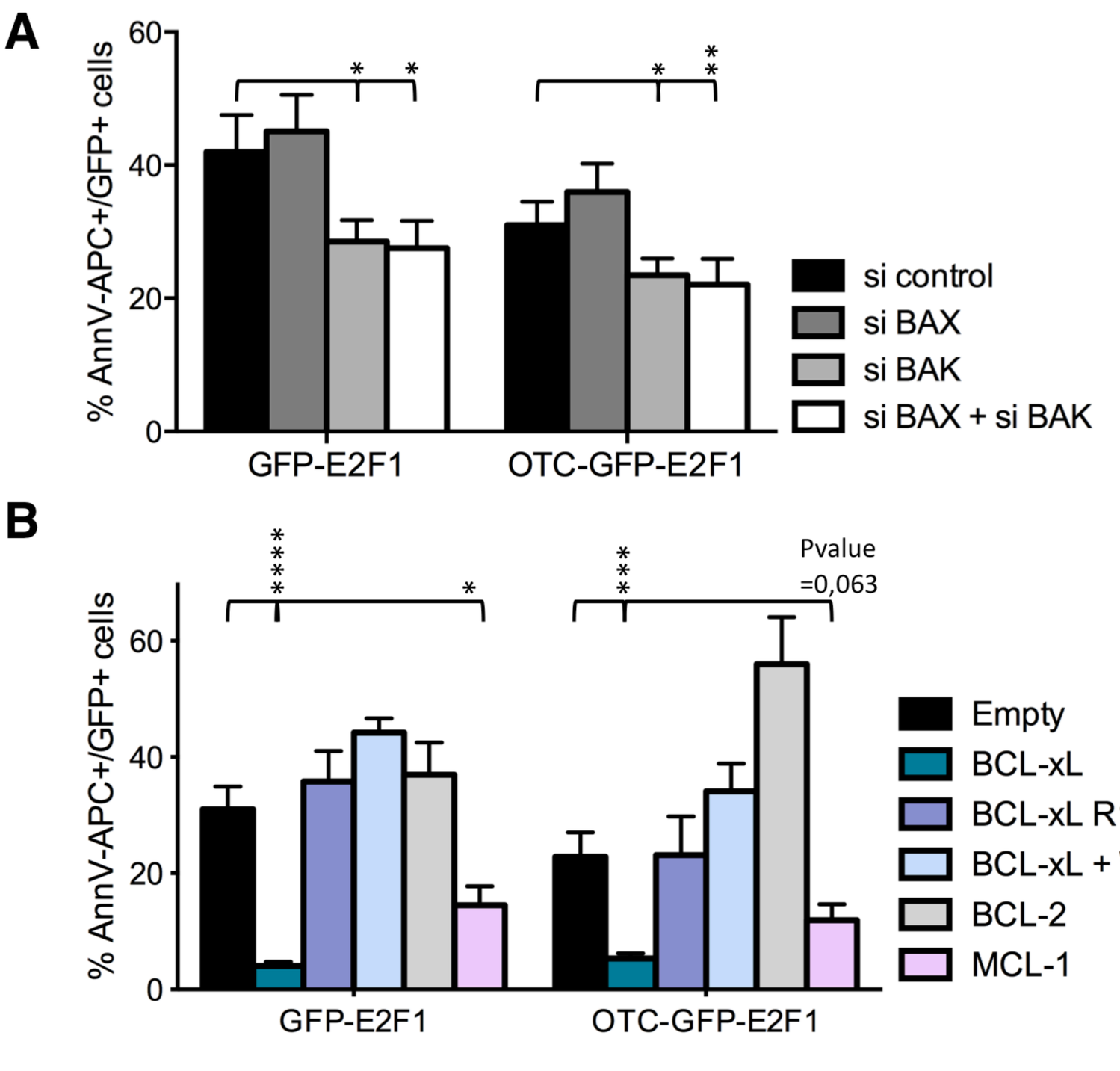
A
% AnnV-APC+/GFP+ cells
60
40
20
0
GFP-E2F1
OTC-GFP-E2F1
si control
si BAX
si BAK
si BAX + si BAK
B
% AnnV-APC+/GFP+ cells
Pvalue
=0,063
60
40
20
0
GFP-E2F1
OTC-GFP-E2F1
Empty
BCL-xL
BCL-xL R139D
BCL-xL + WEHI-539
BCL-2
MCL-1
C
% AnnV-APC+/GFP+ cells
100
80
60
40
20
0
Empty
BAK
BAX
PUMA
PUMA 3A
BIM
tBID
GFP
GFP-E2F1
OTC-GFP-E2F1

Figure 3

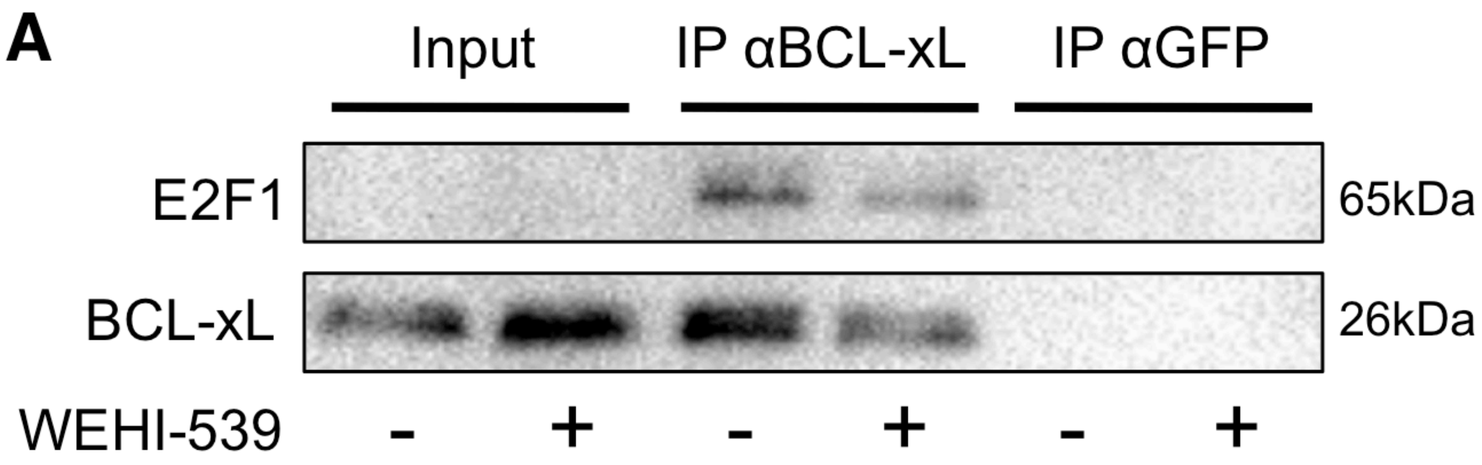
A
Input
IP αBCL-xL
IP αGFP
E2F1
65kDa
BCL-xL
26kDa
WEHI-539
- + - + - +

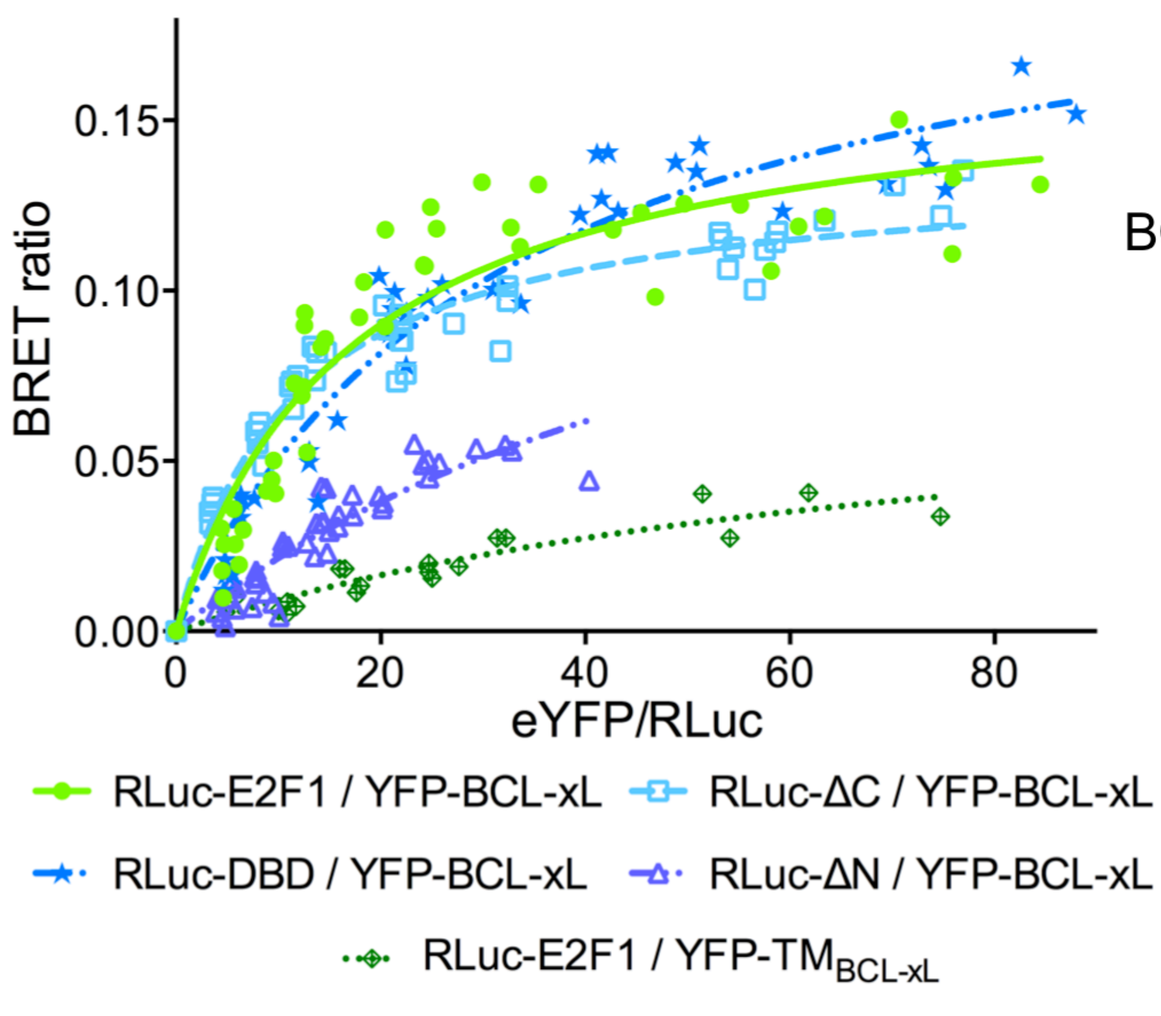
B
BRET ratio
0.00
0.05
0.10
0.15
0
20
40
60
80
eYFP/RLuc
RLuc-E2F1 / YFP-BCL-xL
RLuc-ΔC / YFP-BCL-xL
RLuc-DBD / YFP-BCL-xL
RLuc-ΔN / YFP-BCL-xL
RLuc-E2F1 / YFP-TMBCL-xL

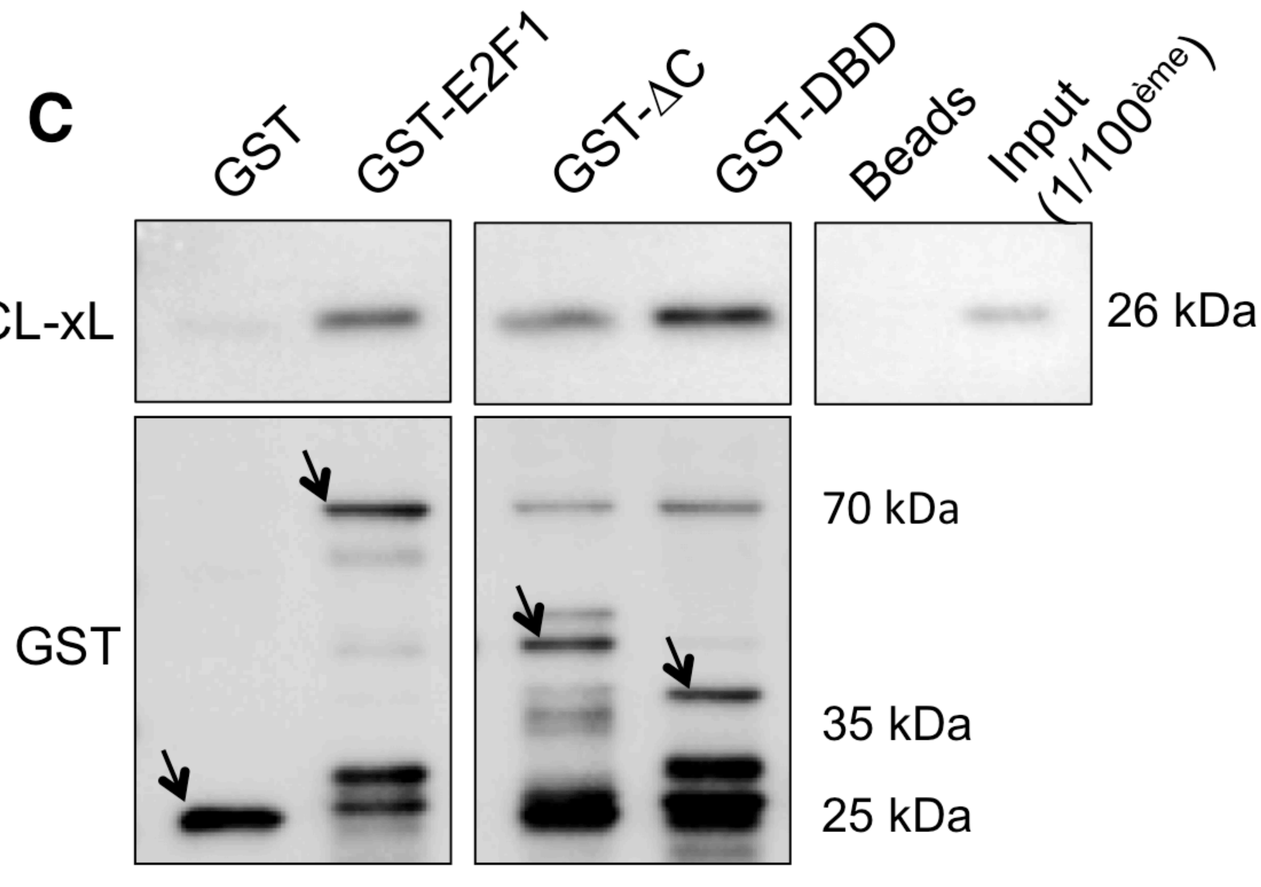
C
GST
GST-E2F1
GST-ΔC
GST-DBD
Beads
Input (1/100ème)
BCL-xL
26 kDa
GST
70 kDa
35 kDa
25 kDa

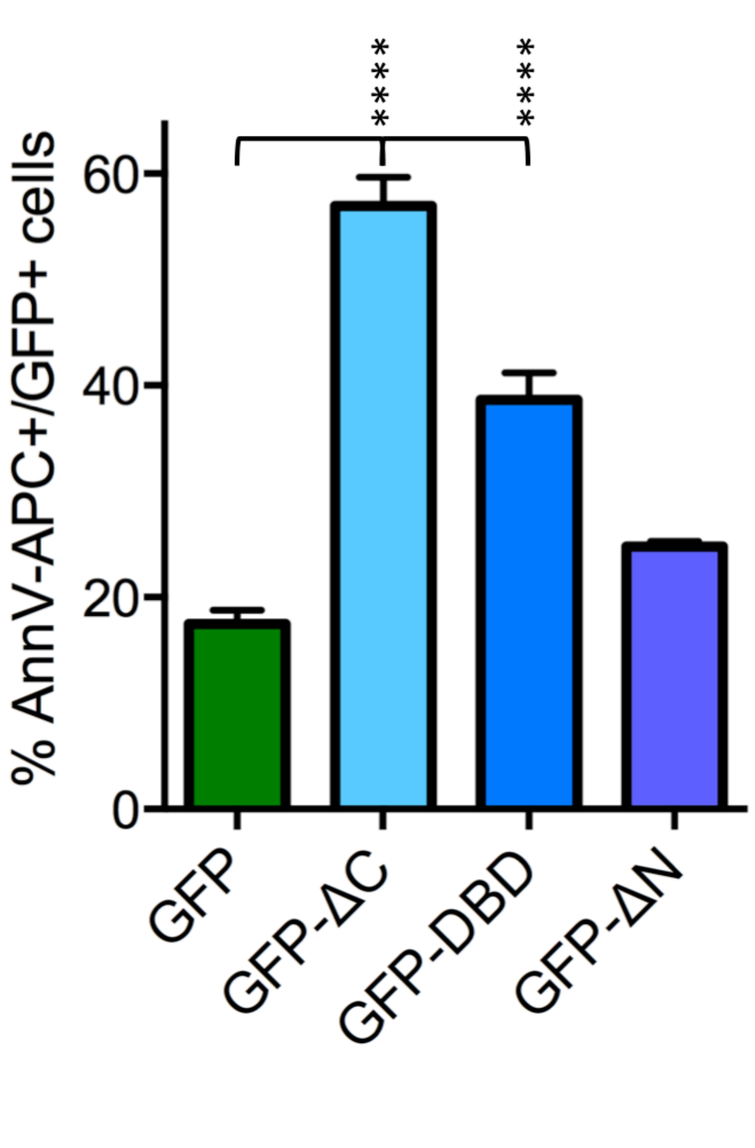
D
% AnnV-APC+/GFP+ cells
0
20
40
60
****
****
GFP
GFP-ΔC
GFP-DBD
GFP-ΔN

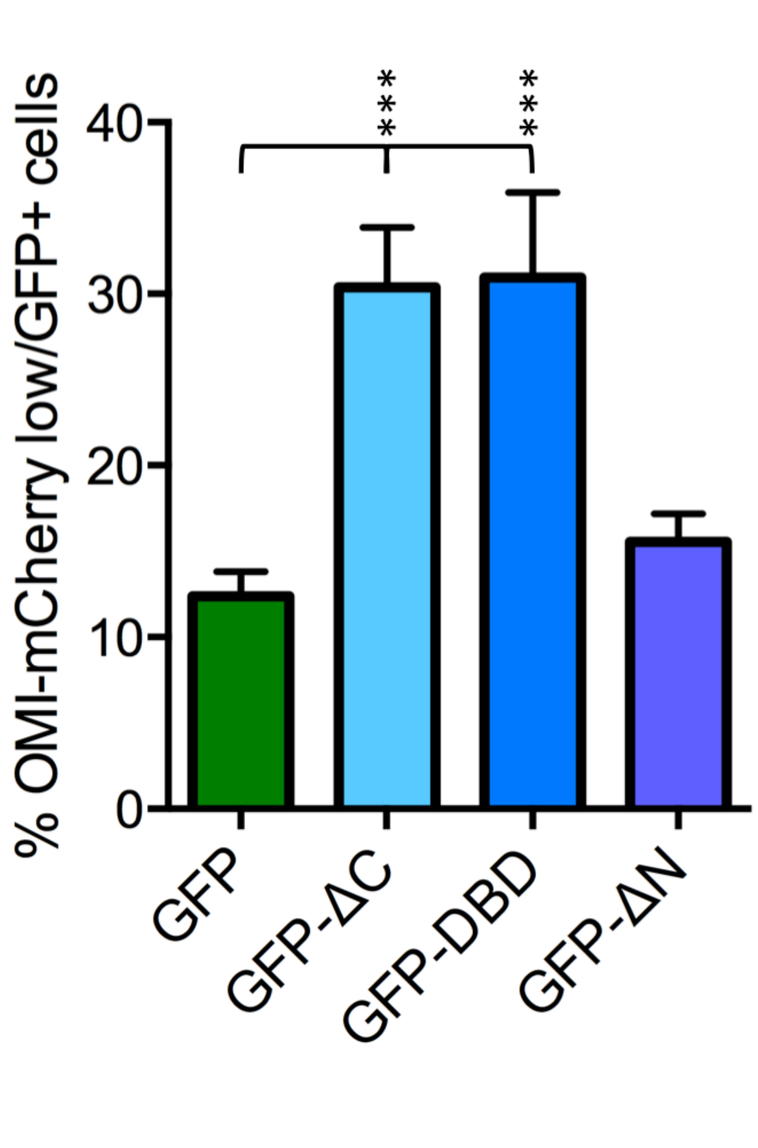
% OMI-mCherry low/GFP+ cells
0
10
20
30
40
***
***
GFP
GFP-ΔC
GFP-DBD
GFP-ΔN

Figure 4

A

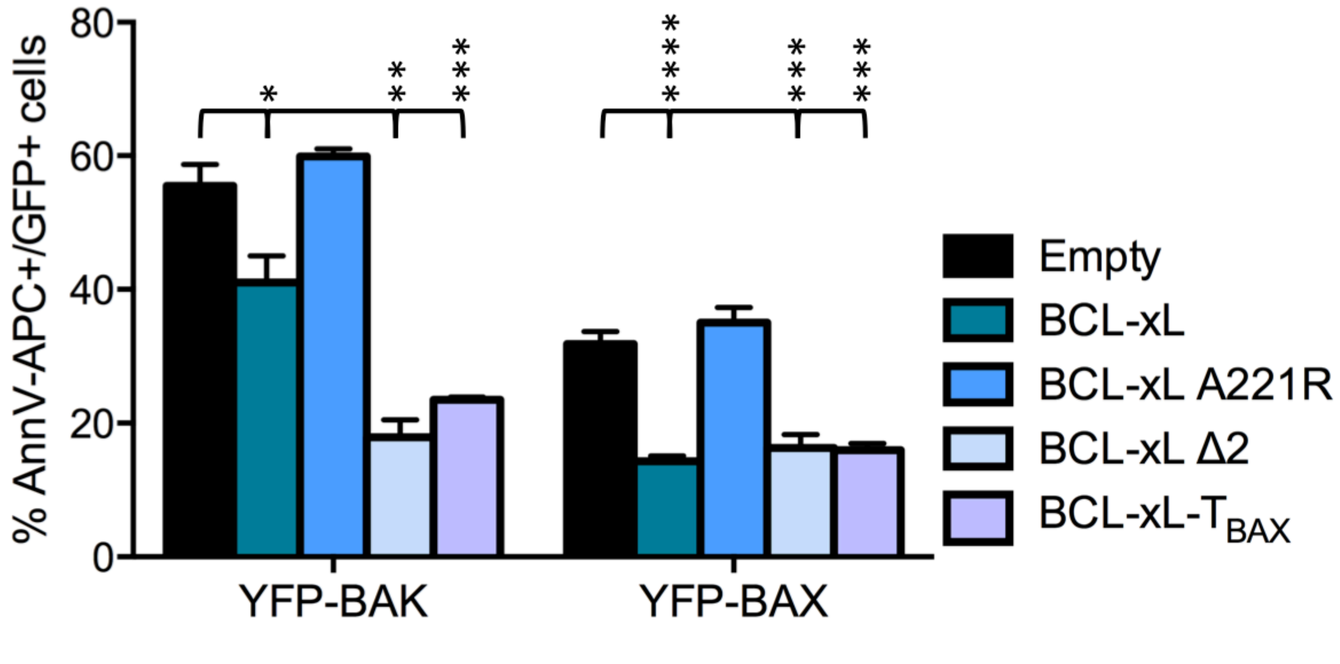
% AnnV-APC+/GFP+ cells
80
60
40
20
0
*
**
***
****
**
***
YFP-BAK
YFP-BAX
Empty
BCL-xL
BCL-xL A221R
BCL-xL Δ2
BCL-xL-T$_{BAX}$

B

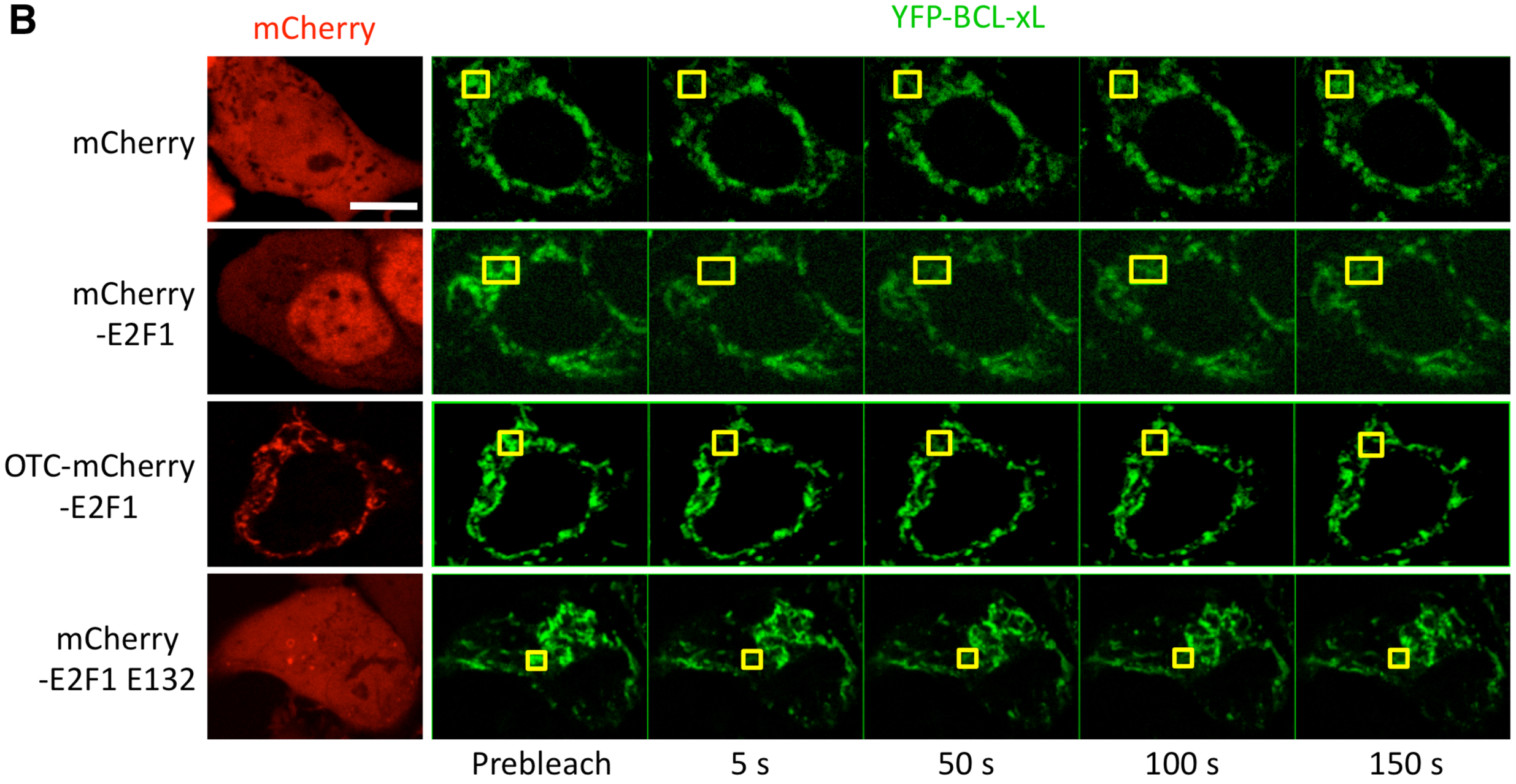
mCherry
YFP-BCL-xL
mCherry
mCherry -E2F1
OTC-mCherry -E2F1
mCherry -E2F1 E132
Prebleach
5 s
50 s
100 s
150 s

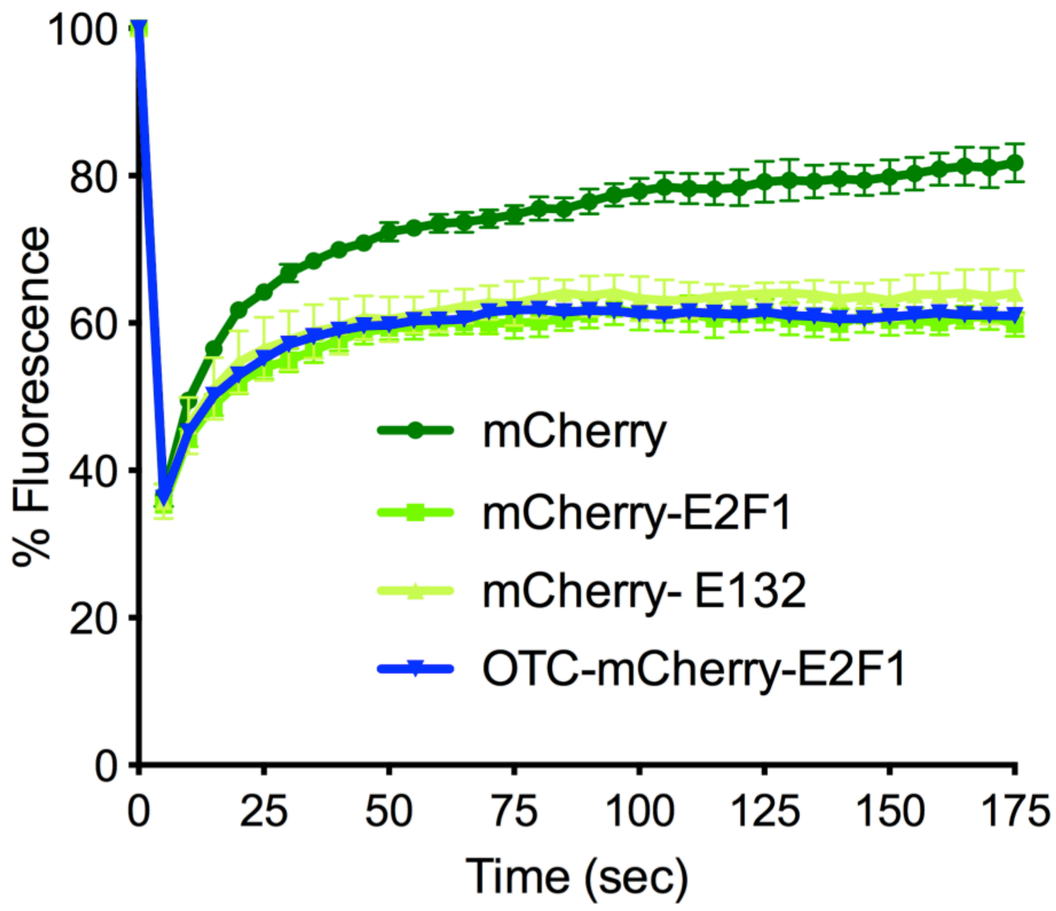
% Fluorescence
100
80
60
40
20
0
0
25
50
75
100
125
150
175
Time (sec)
mCherry
mCherry-E2F1
mCherry- E132
OTC-mCherry-E2F1

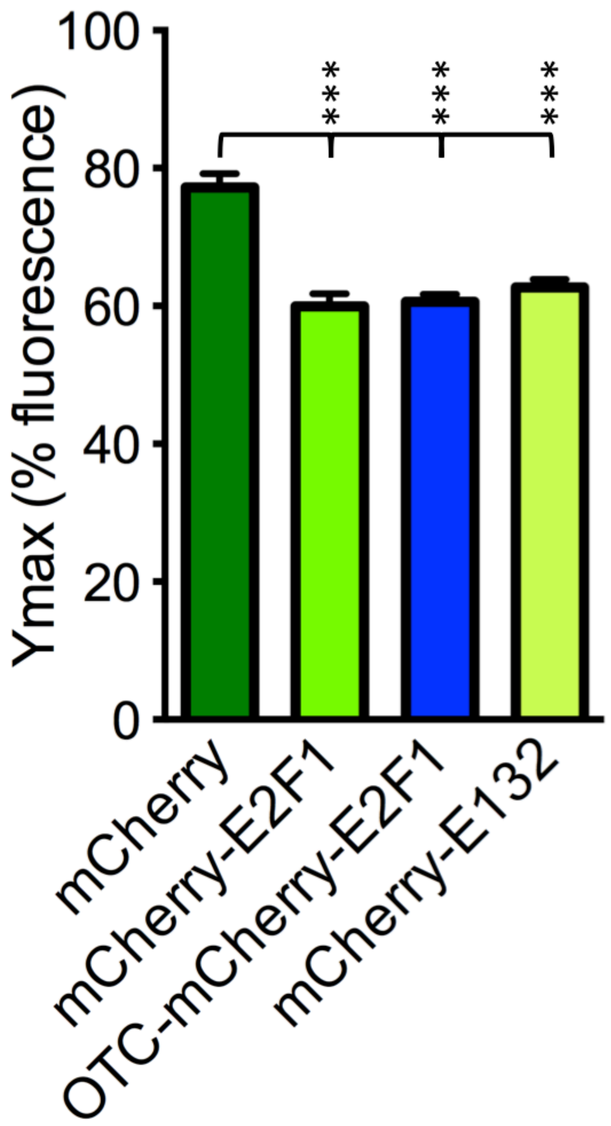
Ymax (% fluorescence)
100
80
60
40
20
0
***
***
***
mCherry
mCherry-E2F1
OTC-mCherry-E2F1
mCherry-E132

Figure EV1

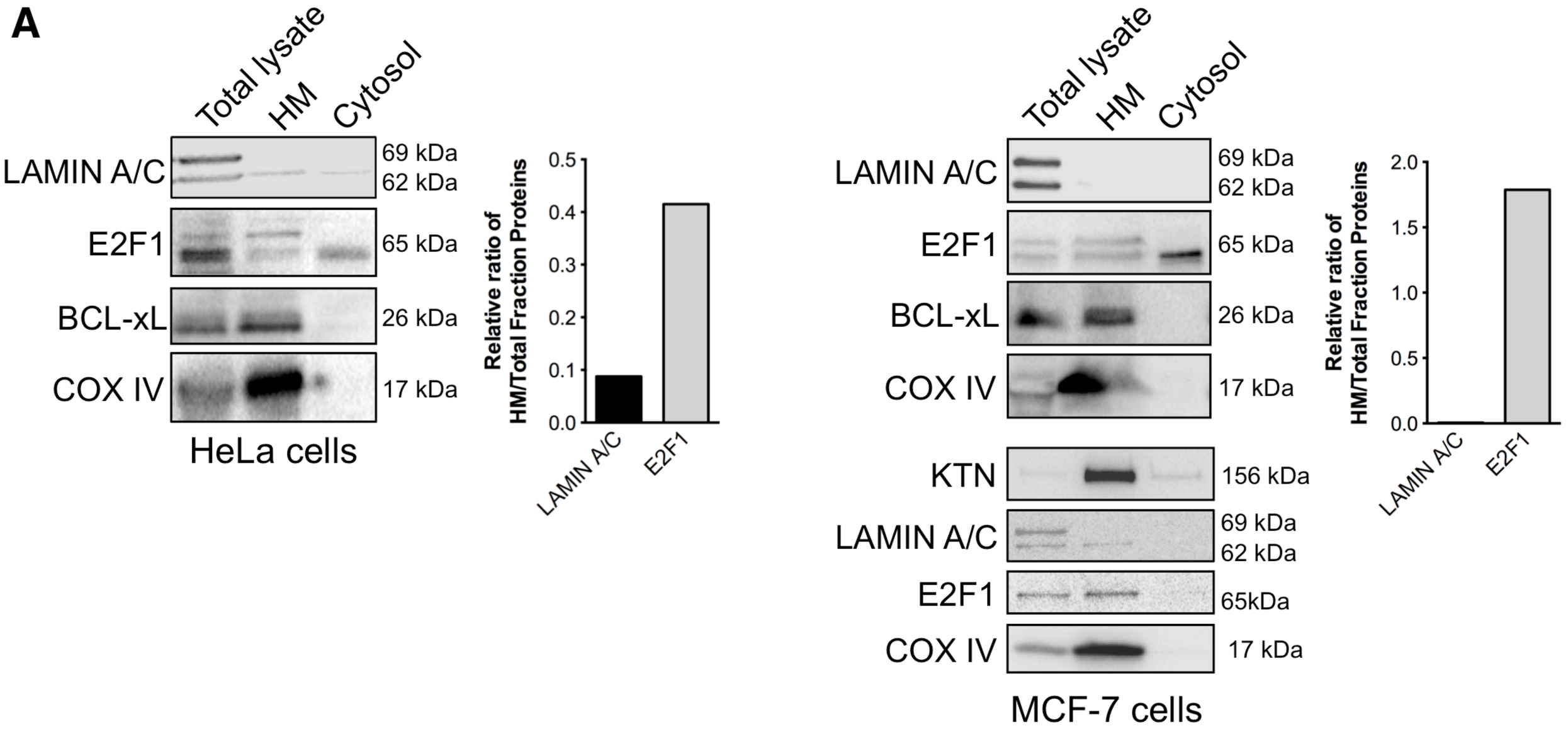
A
Total lysate
HM
Cytosol
LAMIN A/C
69 kDa
62 kDa
E2F1
65 kDa
BCL-xL
26 kDa
COX IV
17 kDa
HeLa cells
Relative ratio of HM/Total Fraction Proteins
0.5
0.4
0.3
0.2
0.1
0.0
LAMIN A/C
E2F1
KTN
156 kDa
65kDa
MCF-7 cells
2.0
1.5
1.0
0.5

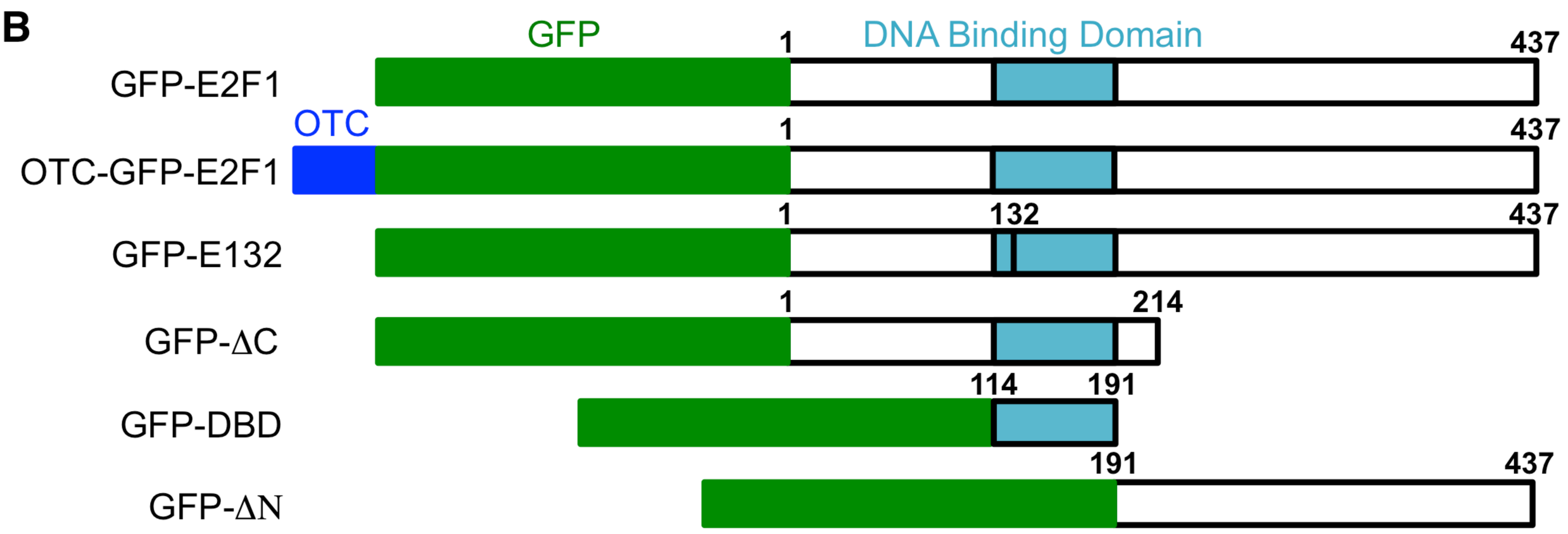
B
GFP
DNA Binding Domain
GFP-E2F1
OTC
OTC-GFP-E2F1
GFP-E132
GFP-ΔC
GFP-DBD
GFP-ΔN
1
437
132
214
114
191

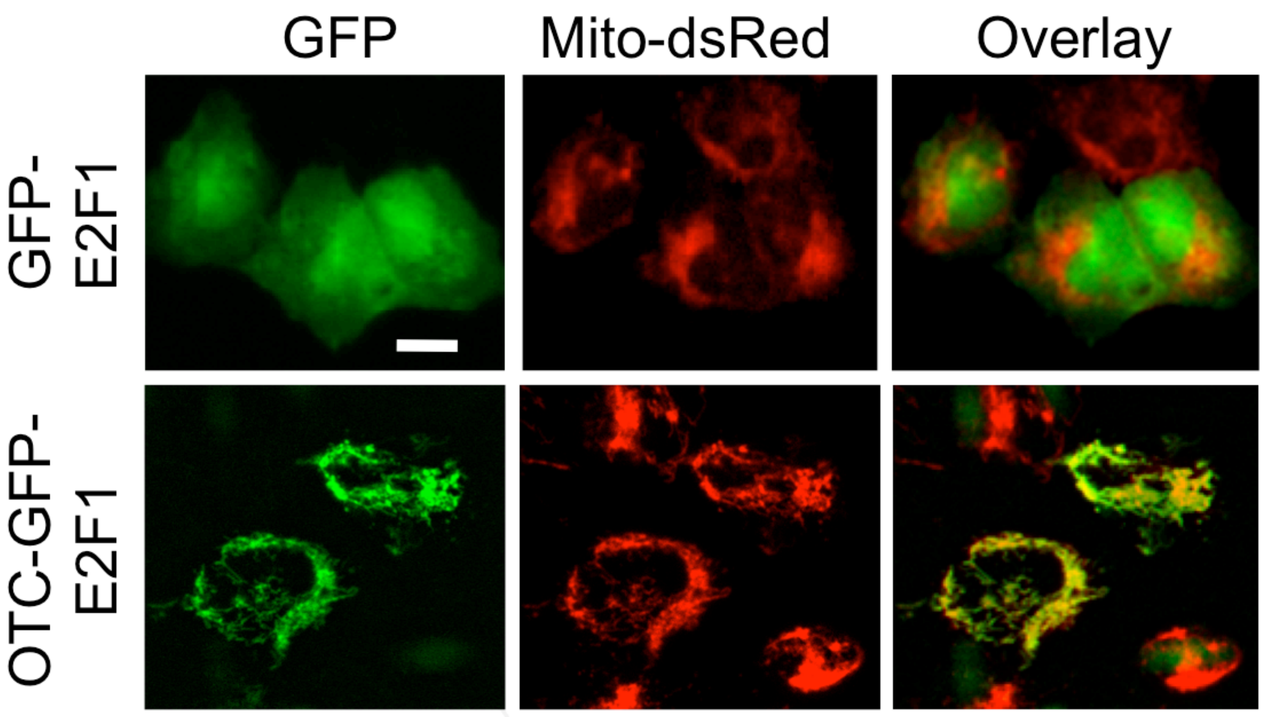
C
GFP
Mito-dsRed
Overlay
GFP-E2F1
OTC-GFP-E2F1

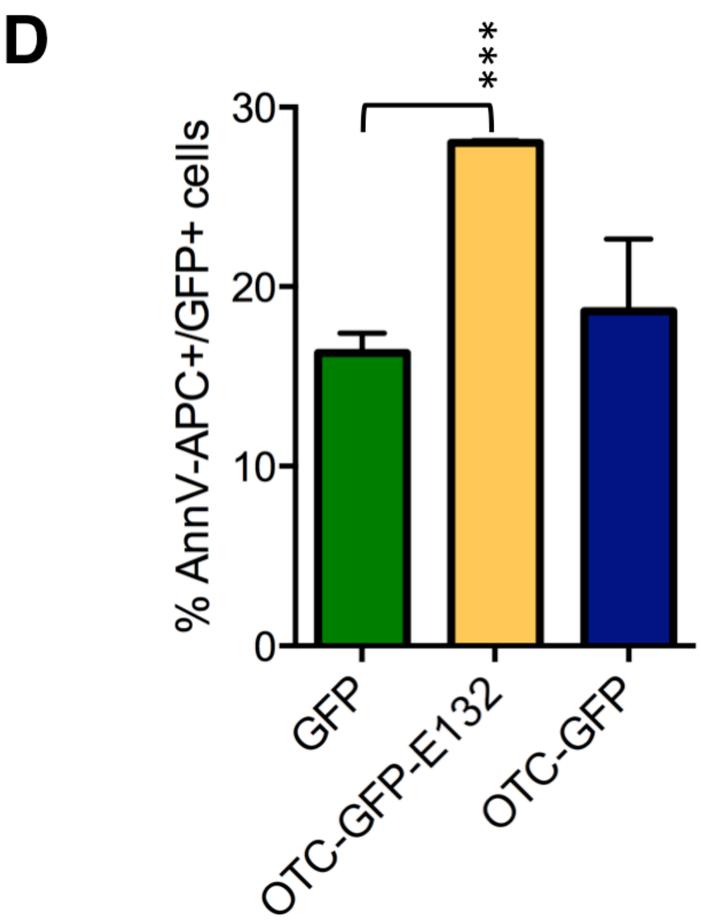
D
***
30
20
10
0
% AnnV-APC+/GFP+ cells
GFP
OTC-GFP-E132
OTC-GFP

Figure EV2

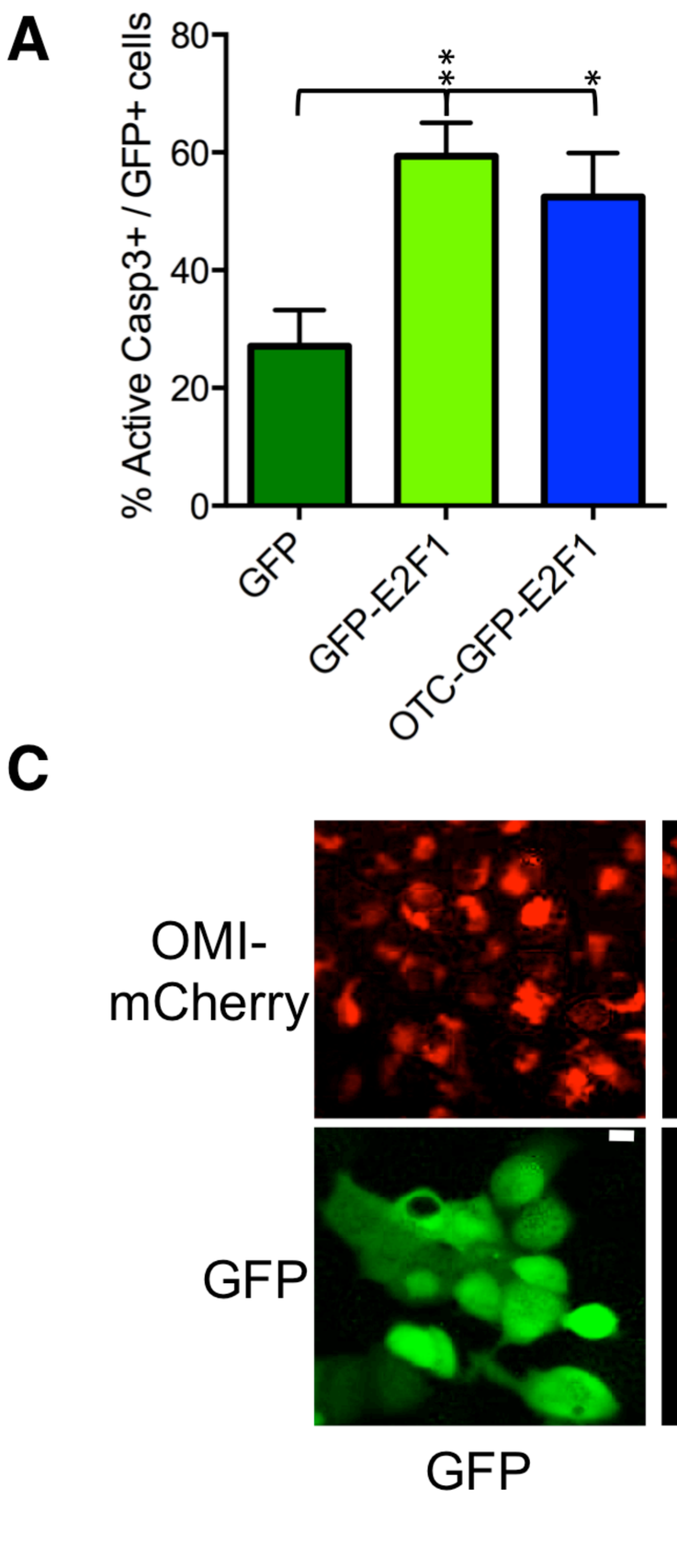
A
% Active Casp3+ / GFP+ cells
0
20
40
60
80
**
*
GFP
GFP-E2F1
OTC-GFP-E2F1

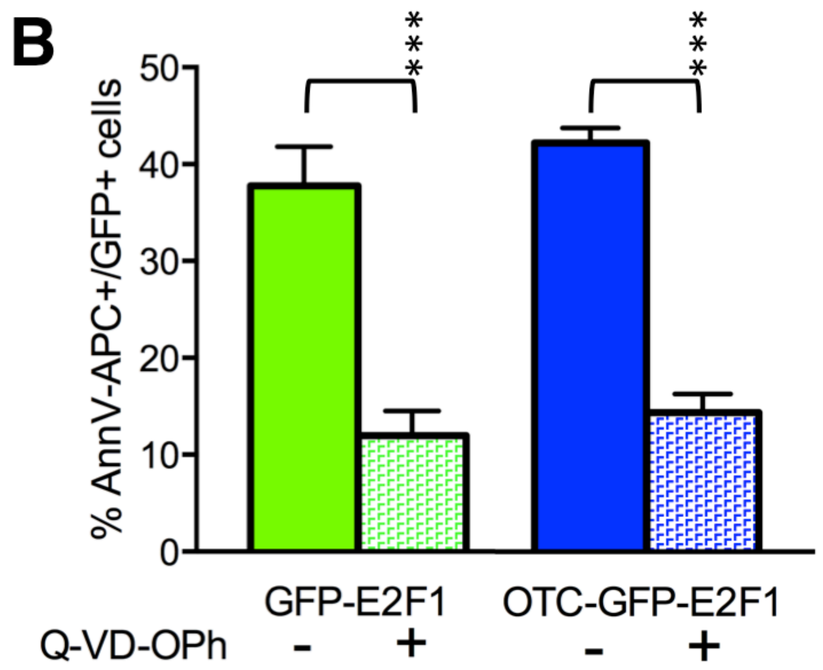
B
% AnnV-APC+/GFP+ cells
0
10
20
30
40
50
***
***
GFP-E2F1
OTC-GFP-E2F1
Q-VD-OPh
-
+
-
+

C
MDA-MB231 OMI-mCherry
OMI-mCherry
GFP
GFP
GFP-E2F1
OTC-GFP
OTC-GFP-E2F1
GFP-E132

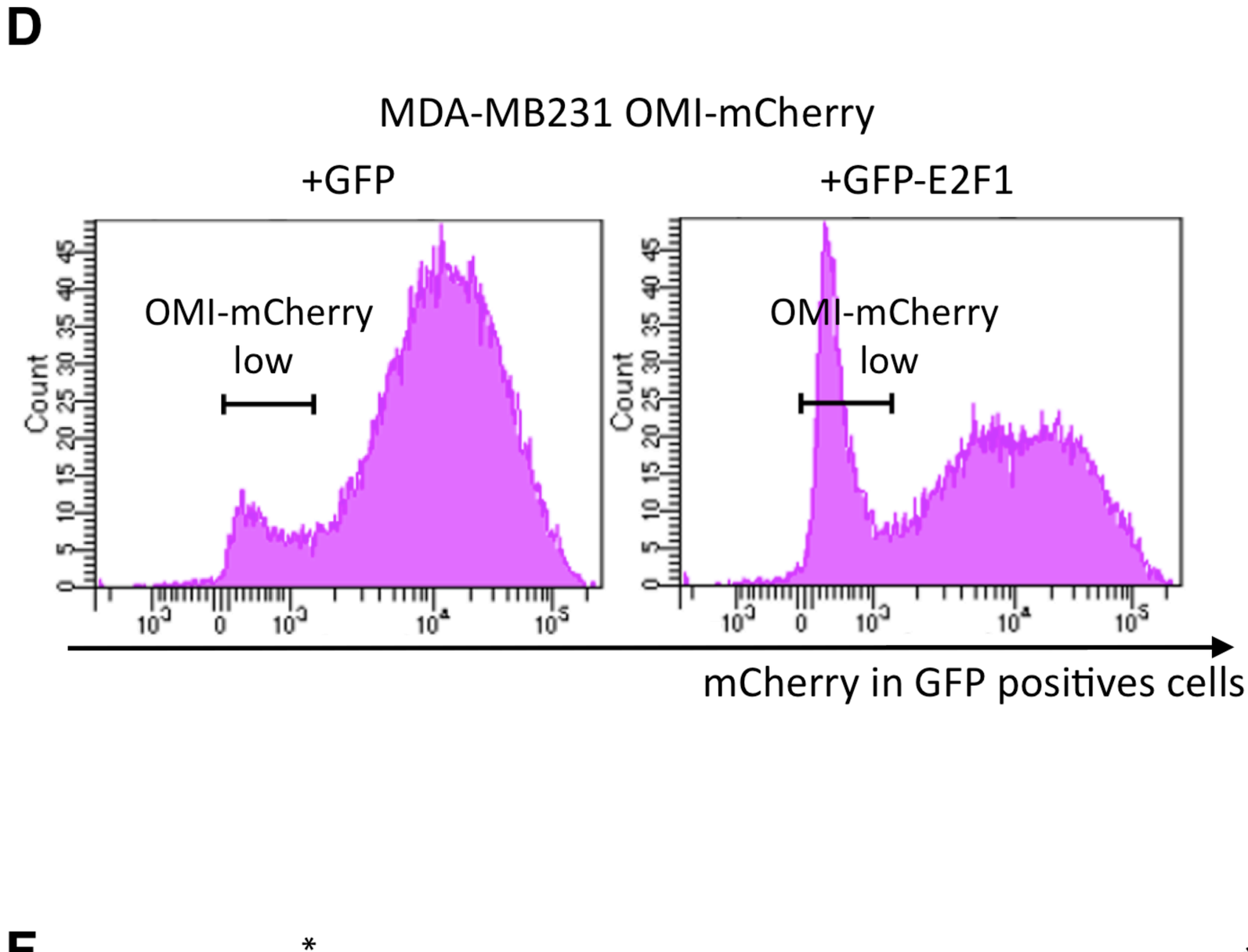
D
MDA-MB231 OMI-mCherry
+GFP
+GFP-E2F1
OMI-mCherry
low
OMI-mCherry
low
Count
mCherry in GFP positives cells

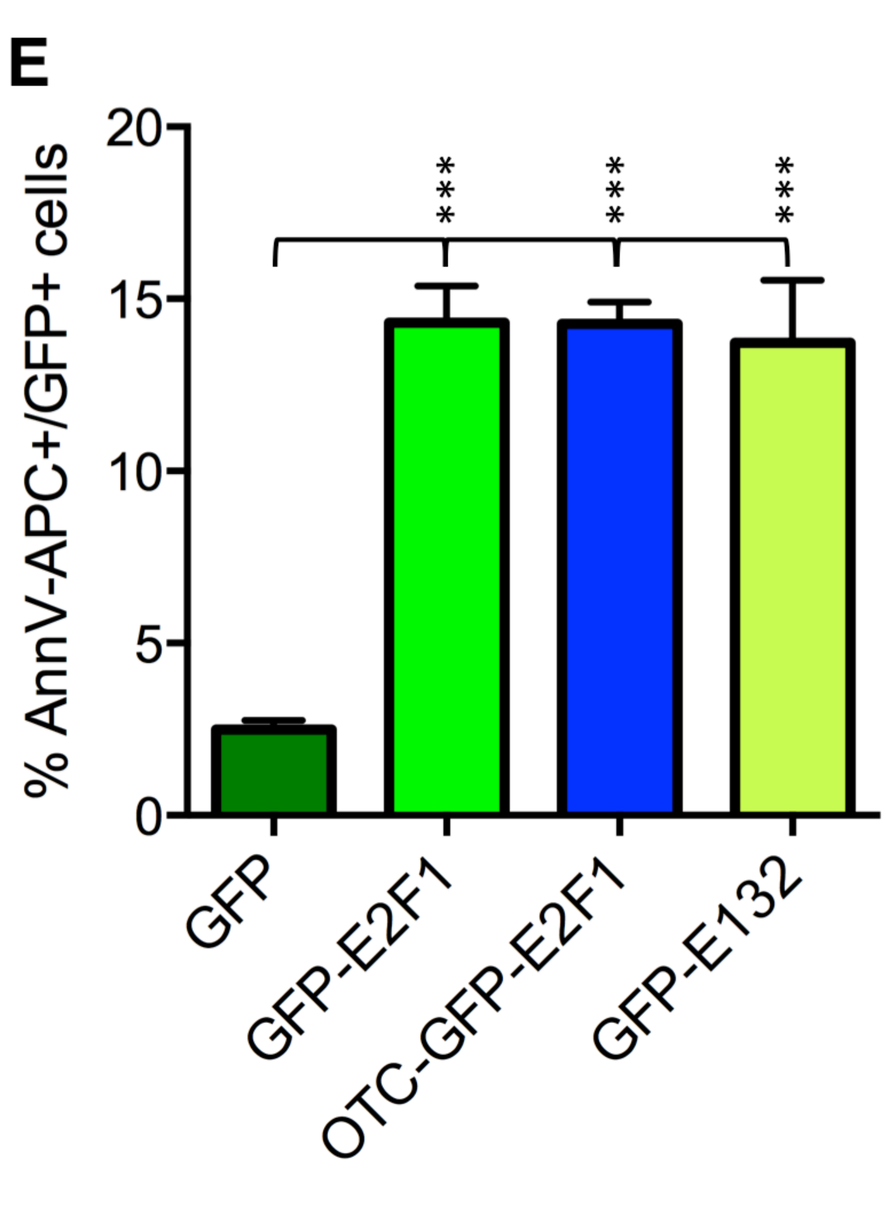
E
% AnnV-APC+/GFP+ cells
0
5
10
15
20
***
***
***
GFP
GFP-E2F1
OTC-GFP-E2F1
GFP-E132

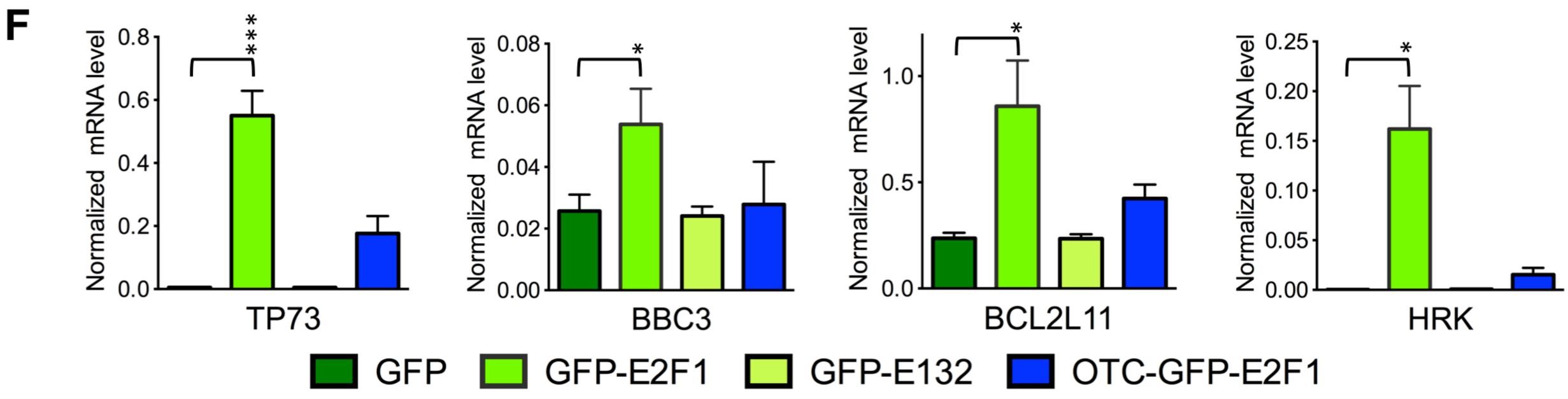
F
Normalized mRNA level
TP73
***
BBC3
*
BCL2L11
*
HRK
*
GFP
GFP-E2F1
GFP-E132
OTC-GFP-E2F1

Figure EV3

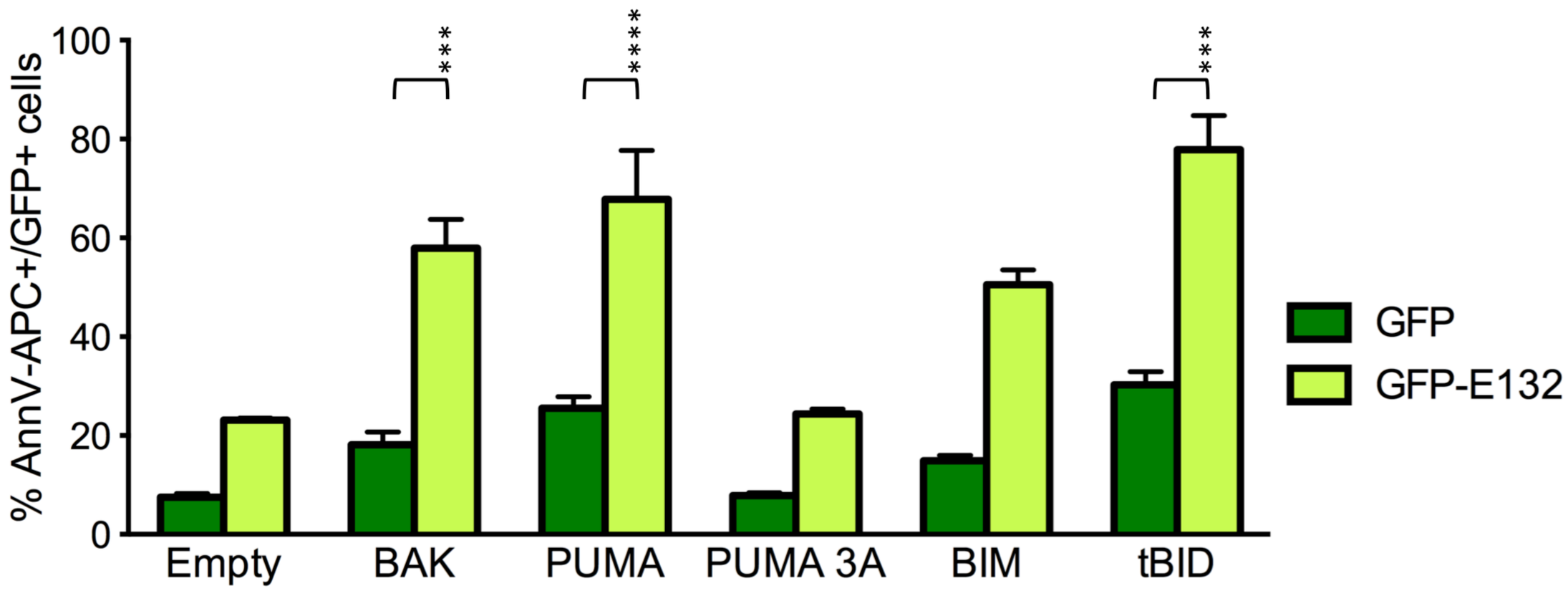
% AnnV-APC+/GFP+ cells
100
80
60
40
20
0
****
****
****
Empty
BAK
PUMA
PUMA 3A
BIM
tBID
GFP
GFP-E132

Figure EV4

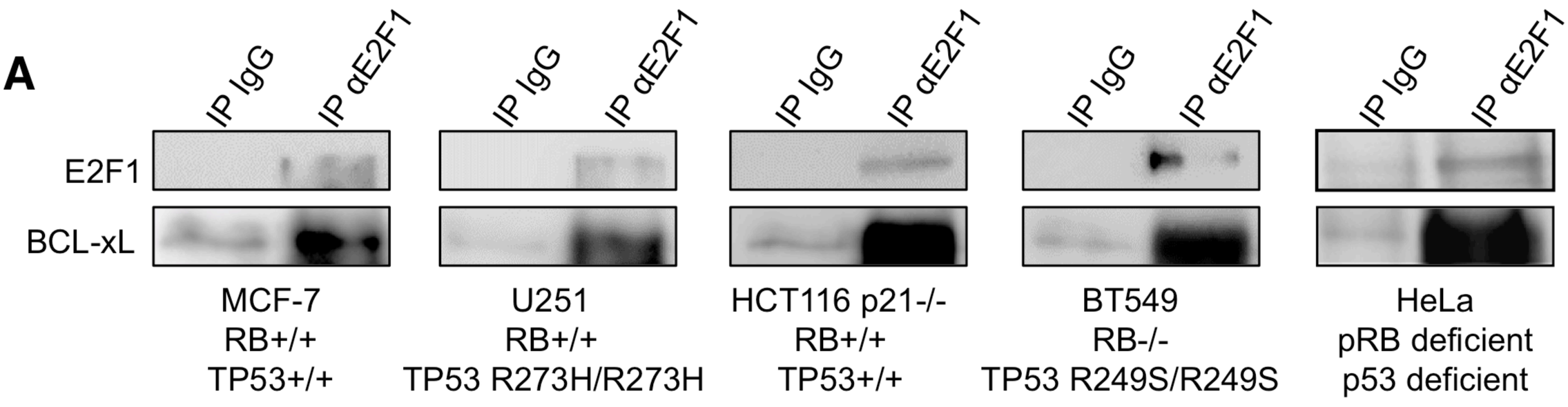
A
IP IgG
IP αE2F1
E2F1
BCL-xL
MCF-7
RB+/+
TP53+/+
U251
RB+/+
TP53 R273H/R273H
HCT116 p21-/-
RB+/+
TP53+/+
BT549
RB-/-
TP53 R249S/R249S
HeLa
pRB deficient
p53 deficient

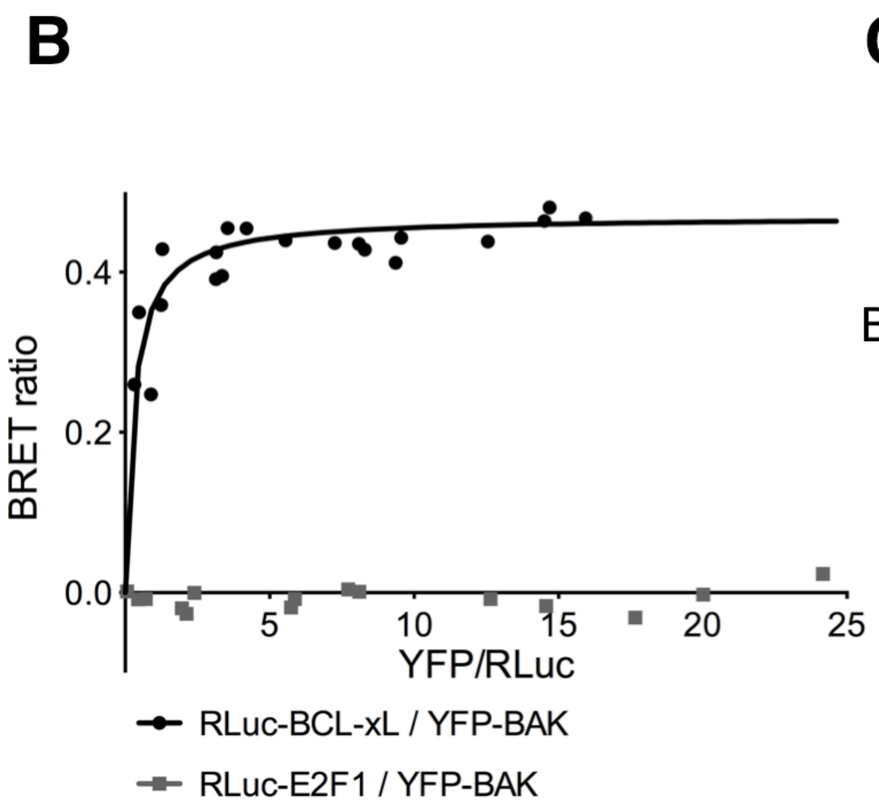
B
BRET ratio
0.0
0.2
0.4
5
10
15
20
25
YFP/RLuc
RLuc-BCL-xL / YFP-BAK
RLuc-E2F1 / YFP-BAK

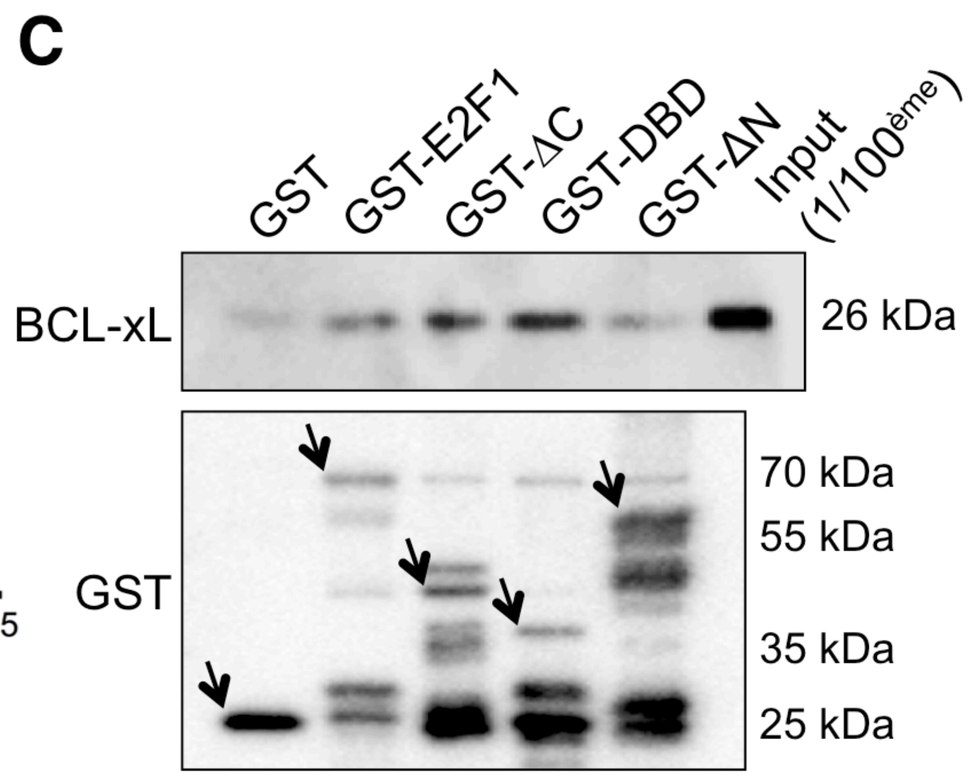
C
GST
GST-E2F1
GST-ΔC
GST-DBD
GST-ΔN
Input (1/100ème)
BCL-xL
26 kDa
GST
70 kDa
55 kDa
35 kDa
25 kDa

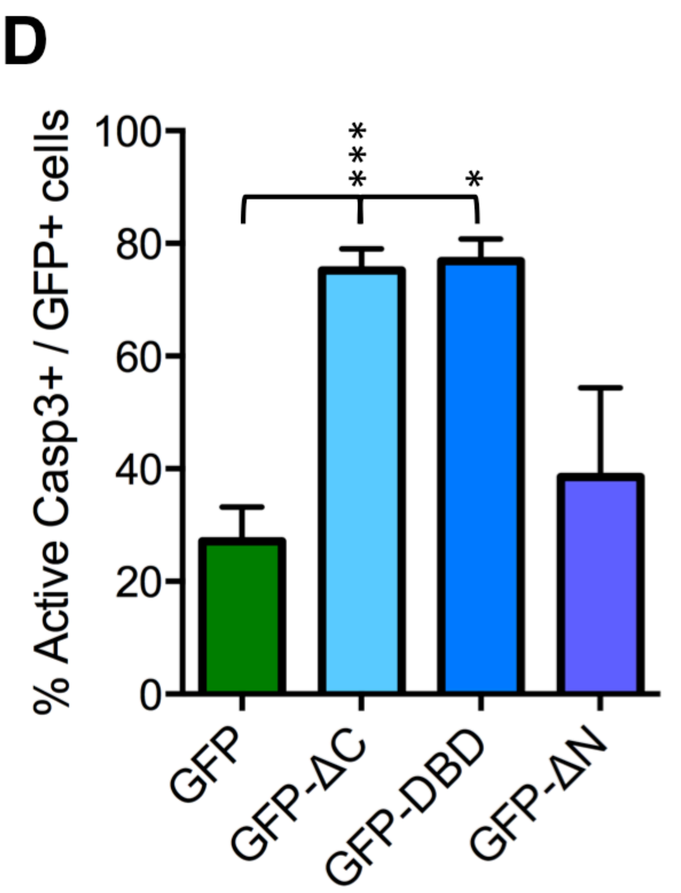
D
% Active Casp3+ / GFP+ cells
0
20
40
60
80
100
***
*
GFP
GFP-ΔC
GFP-DBD
GFP-ΔN

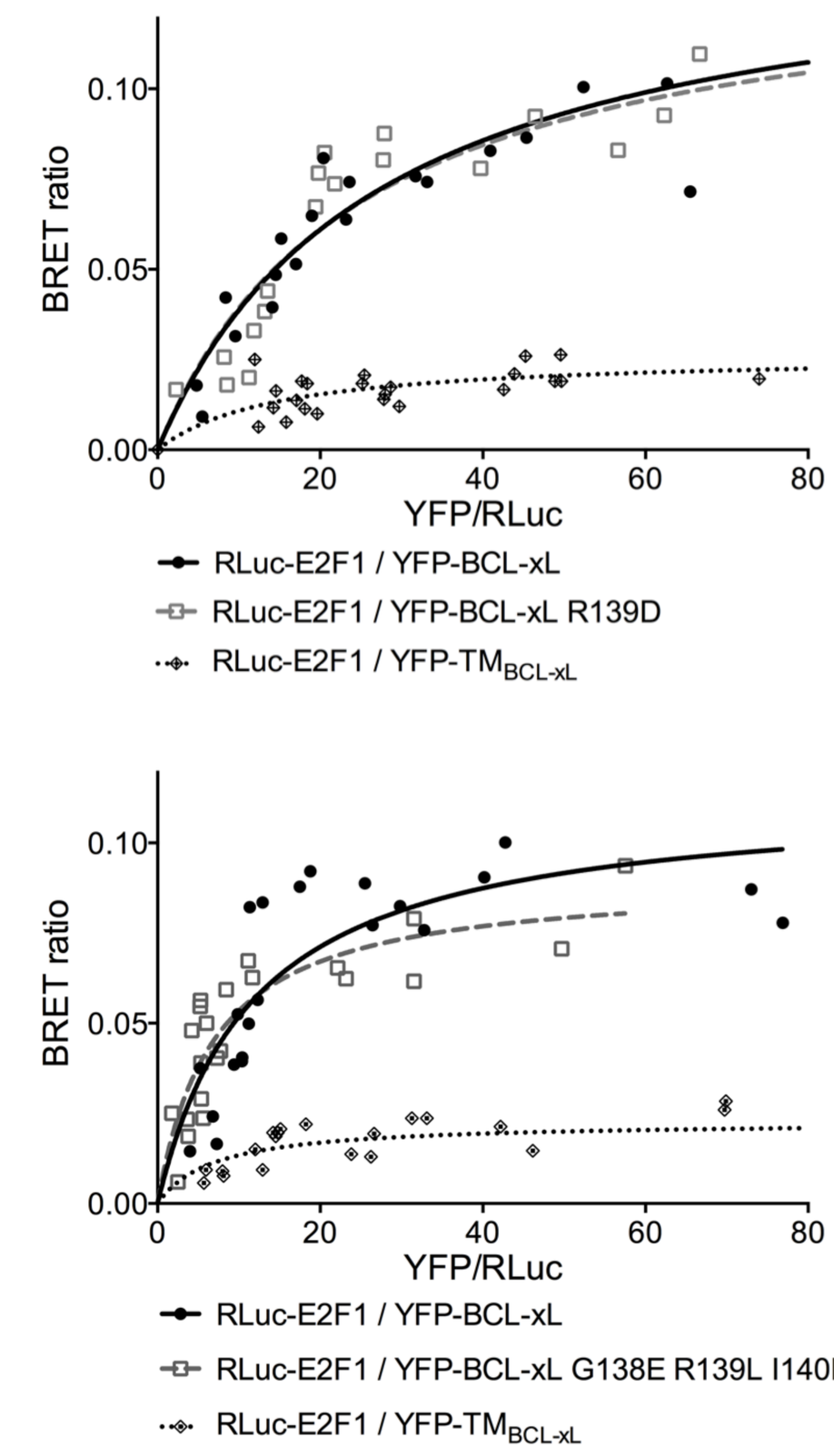
E
BRET ratio
0.00
0.05
0.10
0
20
40
60
80
YFP/RLuc
RLuc-E2F1 / YFP-BCL-xL
RLuc-E2F1 / YFP-BCL-xL R139D
RLuc-E2F1 / YFP-TMBCL-xL
RLuc-E2F1 / YFP-BCL-xL G138E R139L I140N
RLuc-E2F1 / YFP-TMBCL-xL

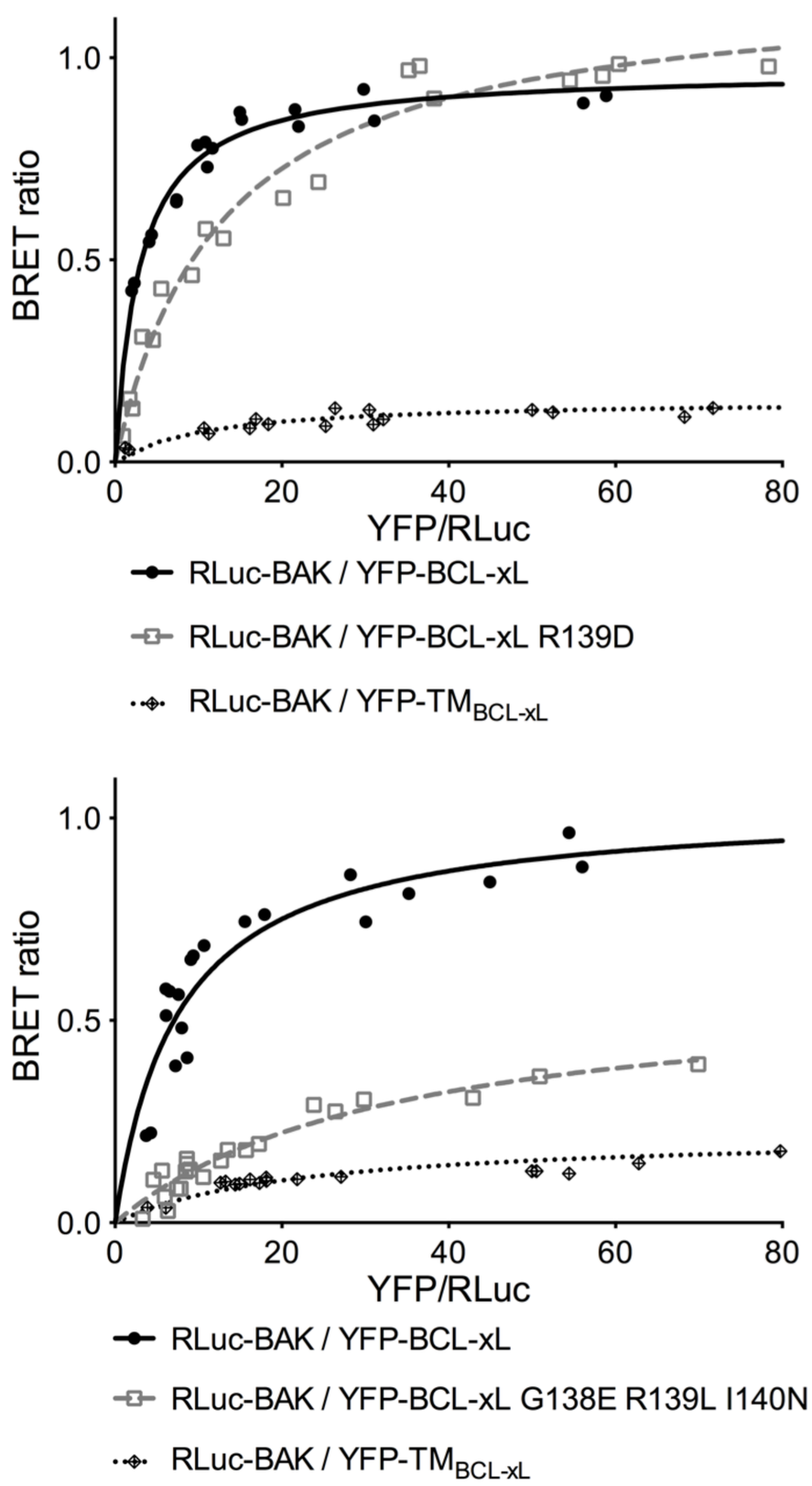
F
BRET ratio
0.0
0.5
1.0
0
20
40
60
80
YFP/RLuc
RLuc-BAK / YFP-BCL-xL
RLuc-BAK / YFP-BCL-xL R139D
RLuc-BAK / YFP-TMBCL-xL
RLuc-BAK / YFP-BCL-xL G138E R139L I140N
RLuc-BAK / YFP-TMBCL-xL

Figure EV5

A

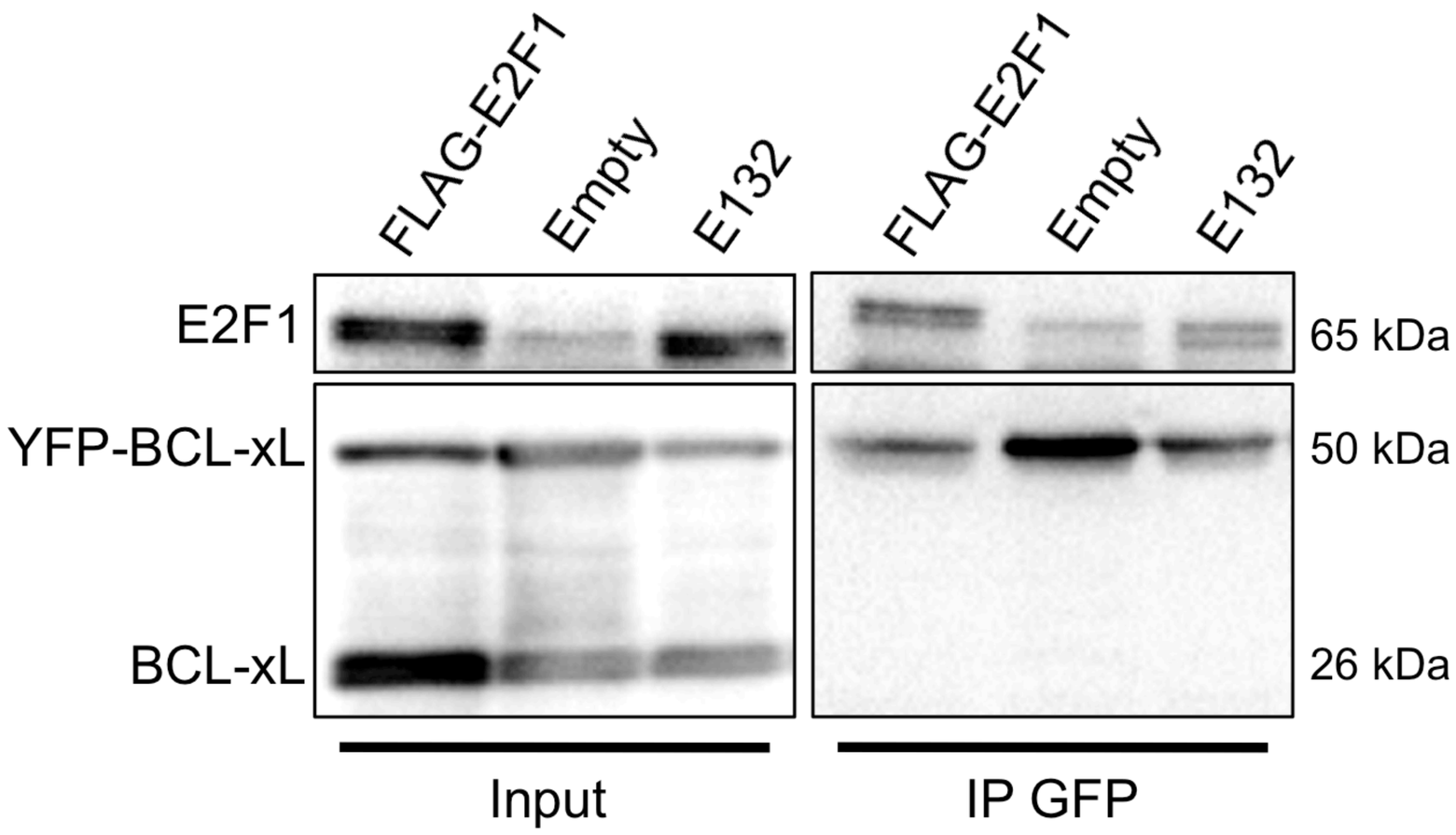

B